

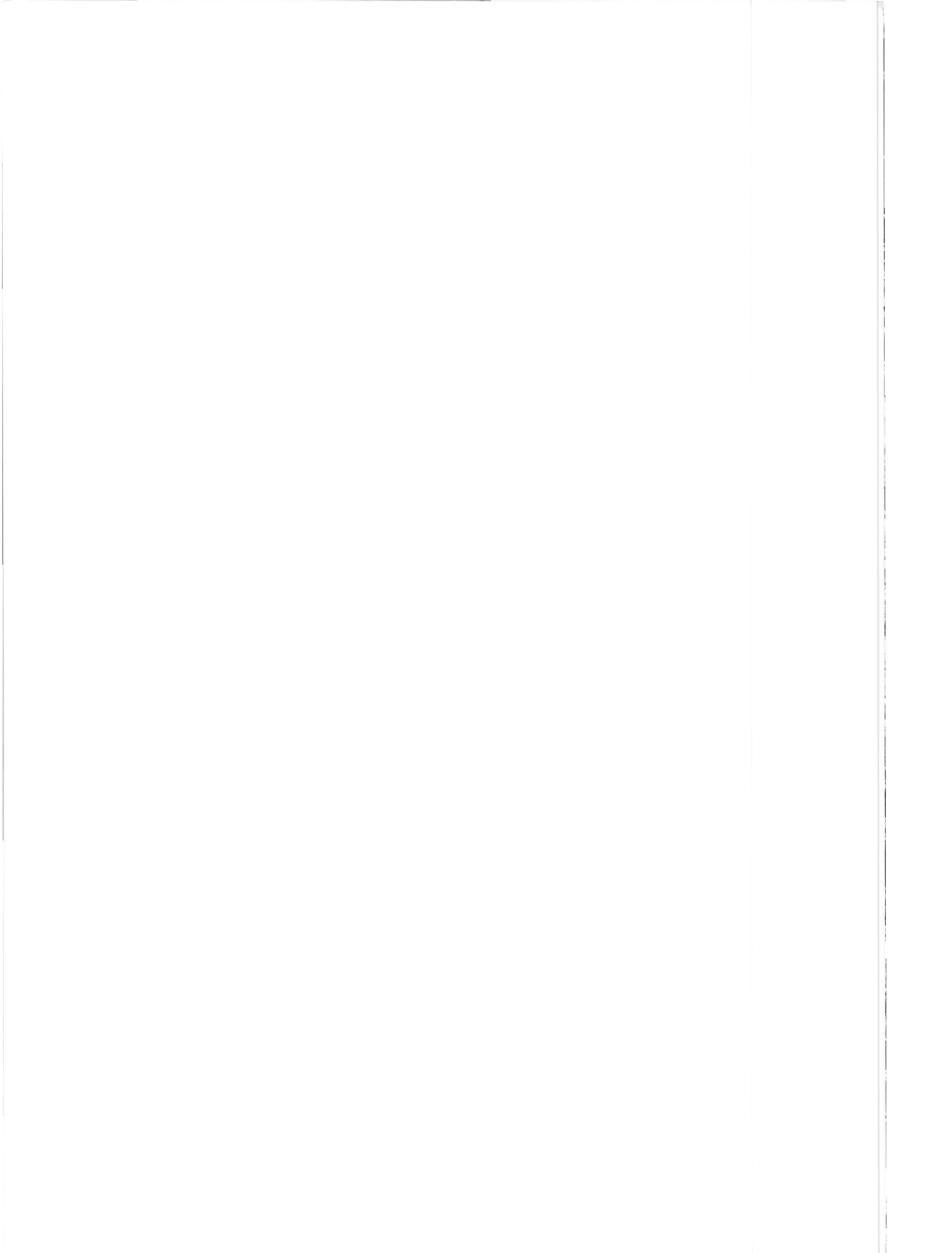
**NRSP-2  
94-02**

RAPPORT  
via  
BIBLIOTHEEK

**Directional ocean wave spectra  
validation:  
ERS-1 SAR and SHIRA**

**H. Greidanus**





**Directional ocean wave spectra validation:  
ERS-1 SAR and SHIRA**

**H. Greidanus  
TNO Physics and Electronics Laboratory**

**bcrs project 1.2/TO-02  
bcrs report 94-02**

**ISBN 90 5411 115 1**

**June 1994**

**This report describes a project, carried out in the framework of the National Remote Sensing Programme (NRSP-2), under responsibility of the Netherlands Remote Sensing Board (BCRS).**

CIP-GEGEVENS KONINKLIJKE BIBLIOTHEEK, DEN HAAG

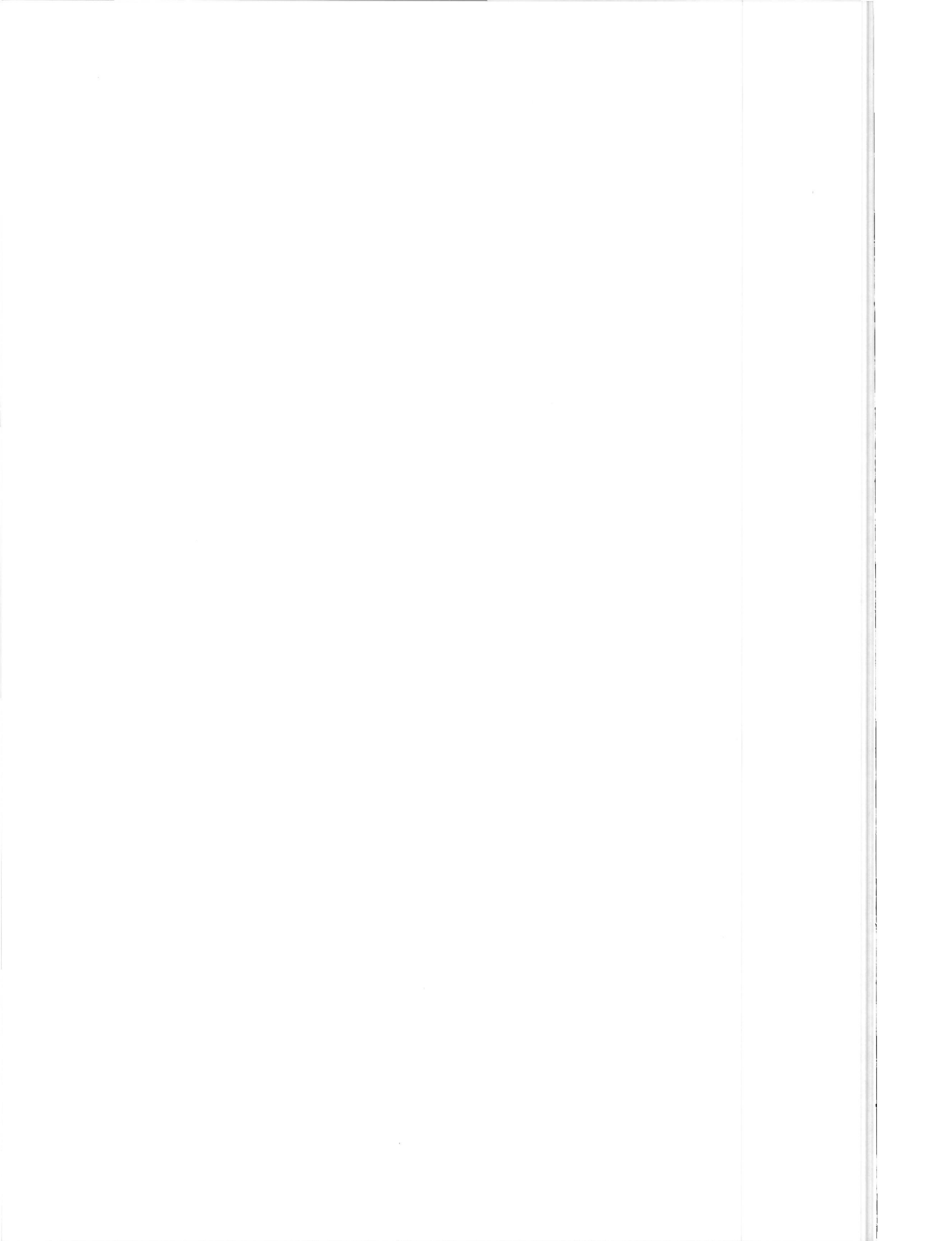
Greidanus, H.

Directional ocean wave spectra validation: ERS-1 and SHIRA /  
H. Greidanus. - Delft : Netherlands Remote Sensing  
Board (BCRS). - Ill. - (BCRS report ; 94-02)  
BCRS project 1.2/TO-02, uitgevoerd in het kader van het  
NRSP-2, onder verantwoordelijkheid van de Beleidscommissie  
Remote Sensing (BCRS). - Met lit. opg.  
ISBN 90-5411-115-1  
Trefw.: oceanografie / remote sensing.

## Abstract

Directional ocean wave spectra as measured by the ERS-1 SAR (Synthetic Aperture Radar) and SHIRA are intercompared. SHIRA is a surface-based X-band (real aperture) imaging radar developed at TNO FEL, used to measure ocean wave spectra with resolution in directional wave number as well as in frequency. The comparison is based on measurements taken on six days during the ERS-1 geophysical calibration/validation campaign in November 1991 over the Norwegian Sea. During the experiment, conditions of strong wind, high sea states and long waves prevailed. For the comparison, the ERS-1 spectra are corrected for stationary instrumental response and speckle noise; no corrections for the radar modulation transfer function are applied.

The ERS-1 SAR spectra compare to the SHIRA spectra in accordance with current SAR wave imaging (velocity bunching) models. The SAR imaging is always in the non-linear domain, and the ERS-1 spectra are dominated by an azimuth cutoff. SHIRA produces much less distorted spectra, and performs much better particularly in detecting the shorter ( $\lambda < 75$  m) waves.



## Contents

<b>Abstract</b>	<b>1</b>
<b>1 Introduction</b>	<b>5</b>
<b>2 Experiment and sensors</b>	<b>5</b>
2.1 Experiment . . . . .	5
2.2 SHIRA . . . . .	6
2.3 ERS-1 SAR . . . . .	7
<b>3 Data Processing</b>	<b>7</b>
3.1 SHIRA . . . . .	7
3.2 ERS-1 SAR . . . . .	9
<b>4 Results</b>	<b>9</b>
4.1 In-situ hydro-meteorological data . . . . .	9
4.2 SHIRA . . . . .	10
4.3 ERS-1 SAR . . . . .	12
<b>5 Discussion</b>	<b>13</b>
5.1 Results of the intercomparison . . . . .	13
5.2 Future work . . . . .	14
<b>References</b>	<b>17</b>
<b>Figures</b>	<b>19</b>



## 1 Introduction

This report concerns the remote measurement of directional ocean wave spectra by two sensors: the ERS-1 SAR (Synthetic Aperture Radar) and SHIRA. In the fall of 1991, the large experimental campaign "RENE 91" was held in the Norwegian Sea. Its purpose was the geophysical calibration and validation of oceanographic measurements of the ERS-1 (European Remote Sensing) satellite. The campaign was organized by ESA (European Space Agency), the operator of the ERS-1. TNO FEL has participated in RENE 91 with two instruments: SHIRA and PHARS. SHIRA is a shipborne radar, developed by TNO FEL for the measurement of ocean wave directional spectra. (It has also been used for other maritime measurements such as oil slick monitoring.) PHARS is an airborne SAR, also developed by TNO FEL, in collaboration with the Netherlands' Aerospace Laboratory and the Delft University of Technology. Both instruments were used to measure the ocean waves, in order to compare the results with those from the ERS-1 SAR (image mode). In addition, buoy spectra and meteorological in-situ data were available.

Purpose of the present report is the intercomparison of SHIRA and ERS-1 derived ocean wave spectra, thereby assessing the geophysical consistency of both sensors. In a number of previous publications partial results of the involvement of TNO FEL with RENE 91 have been presented. In [1] and [2] parts of the wave data sets of ERS-1, PHARS, SHIRA and buoys have been intercompared. In a previous report [3] all the PHARS measurements have been discussed. The present, final report addresses the remaining issue of a complete SHIRA/ERS-1 intercomparison and completes the BCRS sponsored contribution of TNO FEL to RENE 91.

In the previous publications, SHIRA and ERS-1 data have been intercompared to some extent already. Not all of the discussion will be repeated here. In particular, some consideration was given in [3] to the SAR imaging of ocean waves, in order to be able to better interpret the PHARS and ERS-1 data; that discussion pertains to the present analysis as well.

However, there are some differences between the present report and the previous work in the data type and applied analysis. In [1], [2] and [3], ERS-1 Fast Delivery (FD) data were used, while for the present report the Precision product (PRI) was used. The estimation process of the ocean wave spectra used here is more elaborate. (It will be described in section 3.2.) The SHIRA data are presented in a more detailed way in the present report.

The remainder of the report will consist of a description of the experiment and the sensors (section 2) and the data analysis procedures (section 3). The measurements will be presented in section 4 and compared in sections 4.3 and 5. Finally, possibilities for further work will be suggested.

## 2 Experiment and sensors

### 2.1 Experiment

The RENE 91 geophysical calibration/validation campaign was held from mid September to mid December 1991. Purpose was to compare ERS-1 measurements and derived results with other, simultaneous, remotely sensed data and in-situ measurements. Location of the campaign was the Haltenbanken area, on the Norwegian Sea, West of Trondheim, Norway.

Between November 17 and November 29, 1991, SHIRA measurements of directional wave spectra have been made from the German research vessel "Gauss". During this period, ERS-1 imaged the area around the Gauss on 6 occasions, listed in Table 1. Only those SHIRA measurements that were taken concurrently with ERS-1 are explicitly presented; they are added into Table 1. However, all SHIRA measurements made during the whole period were processed and analyzed, in order to check consistency of the data. Location of the Gauss for the six observations concurrent with ERS-1 was near the position designated T10, at  $7^{\circ} 41.79'$  East and  $64^{\circ} 30.08'$  North. At that location a Datawell wave buoy was moored.

During the experiment period, the Gauss has not always been near T10, and SHIRA has made some observations on other locations in the Haltenbanken area.

The locations of the ERS-1 scenes and SHIRA position T10 are plotted in Figure 1. (All figures are in the back of the report.)

Date <sup>a</sup>	ERS-1				SHIRA	
	Time (UT)	Orbit	Frame	Heading <sup>b</sup>	Time (UT)	ID
19	21:10	1803	1305	-16.3° (A)	20:12	g191191e
20	10:48	1811	2295	-163.8° (D)	10:47	g201191e
22	21:10	1846	1305	-16.3° (A)	21:14	g221191j
23	10:48	1854	2295	-163.8° (D)	10:50	g231191e
25	21:10	1889	1305	-16.3° (A)	21:13	g251191f
28	21:10	1932	1305	-16.3° (A)	21:00	g281191i

a: November 1991.

b: Flight (azimuth) direction clockwise from North; Ascending or Descending orbit.

Table 1: Dates and times of ERS-1 and SHIRA measurements.

From Table 1 it can be seen that a SHIRA measurement is available within minutes from each ERS-1 measurement, except on date 19 when there was an hour difference. This is because at the time of that ERS-1 overpass the Gauss was sailing at 10 knots, and although SHIRA spectra are available at 21:13 and 21:16 that day, the motion effects make the intercomparison less straightforward.

In-situ data that were available comprised meteorological measurements on board the Gauss, and ocean wave measurements by the Datawell wave bouy at T10.

On three days during the campaign, the airborne SAR PHARS has measured ocean wave spectra: November 19, 20 and 22, 1991. These measurements were the subject of the previous report [3] and are not discussed here anymore.

## 2.2 SHIRA

SHIRA is a shipborne radar system for oceanographic measurements, in particular directional ocean wave spectra. SHIRA is derived from a normal ship navigation radar. It differs from that by being able to transmit a better defined pulse and using a rotationally stabilized antenna, so that range resolution and azimuth sampling are of better quality. Furthermore, the received signal is logarithmically amplified to obtain a very high sensitivity and dynamic range, and it is digitized and stored on a PC. Due to data rate limitations, only a limited area of the sea surface can be digitized and stored; this area is defined by an interval in range and azimuth, and is typically 1 km sized, at a distance of 500 to 4000 m from the ship. The radar image of this area shows ocean waves, if they are present, because the waves modulate the radar backscatter. When a full wave spectrum is present, all wave components are superimposed, also in the radar image; hence, a Fourier analysis of the radar image will give an estimate of the wave components that are present, i.e. an estimate of the directional wave spectrum. The selected area of the sea is imaged not once but repeatedly, viz. every time the beam of the rotating antenna sweeps over it. This leads to a series of successive images separated by the antenna revolution period, which is approximately one second. This series of images makes up one SHIRA measurement. By performing a Fourier analysis not only with respect to the spatial coordinates but also in time, a frequency spectrum can be obtained in addition to the wavenumber directional spectrum. In the same process the 180° ambiguity that characterizes wave spectra taken from still images is removed.

One measurement takes somewhat over two minutes. Subsequent processing can be done using a PC with an array processor card that is part of the system on board the ship, so that a directional spectrum is available directly after the measurement.

The main parameters of SHIRA are listed in Table 2; the corresponding ERS-1 parameters (next section) are also in this table. SHIRA is described in more detail in [4] and [5].

	SHIRA	ERS-1 SAR
Frequency (GHz)	9.4 (X-band)	5.3 (C-band)
Polarization	HH	VV
Incidence angle ( $^{\circ}$ )	89	23 <sup>a</sup>
Resolution $R \times A$ (m)	$7.5 \times 15^a$	$30 \times 30^b$
Sampling distance (m)	$10 \times 15^a$	$12.5 \times 12.5^b$
Field of view (km)	$1.2 \times 1.2$	$100 \times 100$
Spatial sampling grid	polar	rectangular
Imaged quantity	Log amplitude	Amplitude <sup>b</sup>
Digitization	8 bit	16 bit <sup>b</sup>
Pulse width (ns)	50	64 (after compression)
Compression factor	-	580
Peak power (kW)	25	4.8
PRF (Hz)	570	1640–1720
Antenna length (m)	2.7	10
Distance $R$ (km)	$1.4^a$	$847^a$
Radar velocity $V$ (m/s)	0–3	7500
$R/V$ (s)	-	113
Antenna revolution time (s)	1.1	-

a: Varies over the image; the relevant mean value has been listed.

b: ERS-1 PRI product.

Table 2: System parameters of SHIRA and the ERS-1 SAR.

### 2.3 ERS-1 SAR

The ERS-1 satellite was launched in July 1991. One of its instruments is a SAR (Synthetic Aperture Radar). From orbit, the SAR images the surface of the earth, including ocean surfaces. It has been quite successful in the imaging and measurement of various oceanic processes and features, such as ocean waves, ocean fronts, surface slicks, ships and ship wakes, shallow-sea bottom topography and tidal areas. Many oceanographic results of ERS-1 have appeared in the literature in the last few years.

The main characteristics of the ERS-1 SAR are tabulated in Table 2. A more detailed description of the satellite and its products can be found in e.g. [6] and [7]. The ERS-1 images were obtained in the framework of a PI-ship (AO NL-6).

## 3 Data Processing

### 3.1 SHIRA

One SHIRA measurement produces a data cube of  $128 \times 128 \times 128$  samples, where two coordinates represent polar spatial coordinates on the sea surface (range and azimuth) and the third coordinate is the time. Resolution, sampling and field of view as set during the six measurements of Table 1 are listed in Table 2. Usually, the sampling distance is set at 5 m, in view of the 7.5 m range resolution. However, in order to better match the very long waves that occurred during this experiment, image size and sampling distance were doubled.

This setup has as a disadvantage that it causes potential aliasing problems with the shorter waves.

The polar sampling is converted to a rectangular grid by nearest neighbor interpolation. Some of the curved and triangular fringes are discarded in the process. The cartesian-sampled 3-dimensional dataset  $I(x, y, t)$  that results can be interpreted as the logarithm of an uncalibrated radar cross section ( $\sigma^0$ ) measure of the sea surface as a function of space  $(x, y)$  and time  $t$ . This data cube is Fourier transformed over all 3 dimensions, and the modulus is taken. This produces an estimate  $F(k_x, k_y, f)$  of the wave spectrum, with  $\vec{k} = (k_x, k_y)$  the wavenumber vector ( $k = |\vec{k}| = 2\pi/\lambda$ ), and  $f$  the wave frequency.

Formally, the ocean wave height spectrum is defined as the Fourier transform of the autocorrelation function of the sea surface height [8], which is equivalent to the expectation value of the squared modulus of the Fourier transform of the surface height. The image spectrum of an imaging radar is related to the wave height spectrum by a so-called modulation transfer function (MTF), which relates the strength of each Fourier component in the sea surface height to the strength of the same Fourier component in the image modulation [9, 10]. For SHIRA, however, no MTF is explicitly known. Nevertheless, past experiments in which SHIRA spectra were compared to other sensors (in particular wave buoys) have shown that the MTF is not strongly dependent on wavenumber (magnitude or direction), i.e. SHIRA spectra agree well with wave spectra from other sensors as far as the relative distribution of wave energy is concerned. However, in the absolute sense SHIRA spectra are uncalibrated: the wave spectra are only measured except for a proportionality constant. Thus, no significant wave height can (yet) be derived from a SHIRA measurement. In the light of these considerations, for the purpose of the present analysis  $F(k_x, k_y, f)$  will be interpreted as the SHIRA ocean wave spectrum.

Several types of spectra may be derived from  $F(k_x, k_y, f)$  by integration over its coordinates. For the present purpose, the directional spectrum  $F(k_x, k_y)$  is most suitable, which is the integral of  $F(k_x, k_y, f)$  over  $f$ . Within the data cube  $F(k_x, k_y, f)$ , the wave energy of the gravity waves is distributed on a 2-dimensional surface: the gravity wave dispersion relation,

$$2\pi f = \sqrt{gk} + \vec{k} \cdot \vec{u}. \quad (1)$$

Here,  $g$  is the gravitational acceleration and  $\vec{u}$  is the advection velocity of the water. (Measuring from a ship that is not drifting but sailing will result in a non-zero  $\vec{u}$ .)

All energy that is present in the 3-D spectrum but does not fall on the dispersion relation does not represent gravity waves. This kind of spectral component can be e.g. harmonics or sub-harmonics, coupled waves, or wind driven features. Although the directional spectrum  $F(\vec{k})$  is the most compact way to present the measurements, it does not show anymore whether the spectral energy satisfies the dispersion relation. Therefore, the SHIRA data are presented here as directional spectra within a frequency band:

$$F(\vec{k}; f_i) = \int_{f_i - \Delta f}^{f_i + \Delta f} F(\vec{k}, f) df. \quad (2)$$

A bandwidth ( $2\Delta f$ ) of 21 mHz was chosen. (In the previous report [3] the SHIRA data were presented in the form  $F(\vec{k})$ .)

In this way, the true gravity wave component can be readily distinguished. Considering the spatial and temporal resolution and sampling (Table 2), and taking into account the wave dispersion relation, no gravity wave spectral energy in  $(k_x, k_y, f)$ -space is expected in the region  $f > 460$  mHz ( $\lambda < 7.5$  m), while for  $290 < f < 460$  mHz ( $7.5 < \lambda < 18.5$  m) the spectra may actually be subject to wave number aliasing. For  $f < 26$  mHz ( $\lambda > 2350$  m), all gravity wave spectral energy is expected to fall in the central wave number bin. It is in the region  $26 < f < 290$  mHz ( $18.5 < \lambda < 2350$  m) where the gravity waves are optimally resolved with the present settings.

### 3.2 ERS-1 SAR

The ERS-1 SAR images have been processed at the UK PAF. The Precision Image product (ERS-1.SAR.PRI) has been used, in contrast to the data used previously [1,2,3] which were Fast Delivery Image Copy (ERS-1.SAR.FDC). The main differences between the two are in sampling and calibration. The FD data have a sample spacing of  $20 \times 15.8$  m (range  $\times$  azimuth) as opposed to the PRI data sampling distance of  $12.5 \times 12.5$  m. The FD data have no calibration, whereas the PRI data are corrected for range spreading loss and antenna elevation pattern.

Several authors have proposed ways to estimate true wave height or wave slope spectra from SAR imagery, based on models of the SAR wave imaging mechanism, e.g. [11], [12], [13], [14] and [15]. Here, the following procedure was used, which is along the lines of [11].

The ERS-1 PRI scenes were divided into  $7 \times 7$  adjacent sub-images of  $1024 \times 1024$  pixels, leaving a symmetric border of some 450 pixels on all sides of the total PRI image unused. The pixel values in each sub-image were squared to go from amplitude to power ( $\propto \sigma^0$ ). This restores the sum of three non-overlapping power-detected looks, because the PRI product is the square root of that [7]. Each sub-image was Fourier transformed, and modulus-squared. The results from all sub-images were added together. Apart from a proportionality constant and the value at the origin, the result represents the speckled SAR image modulation spectrum.

In many spectra disproportionately large values occurred around the origin, due to DC and baseline effects or large scale features in the images. To suppress these large values, the central  $7 \times 7$  spectral pixels were set to zero.

As the next step, the spectra were smoothed with a hanning function of 4 points FWHM, in order to further reduce the noise in the spectra. Each point in the spectrum of a single sub-image, before averaging or smoothing, can be treated as a random variable with a  $\chi_2^2$  distribution, i.e. a  $\chi^2$  distribution with 2 degrees of freedom. This means that such points have a S/N (signal-to-noise) ratio of 1 [12]. Averaging and smoothing multiplies the number of degrees of freedom by the number of independent measurements, so that the averaging over the 49 subimage-spectra results in a  $\chi_{98}^2$  distribution for the spectral points (S/N=7), and the subsequent smoothing (equivalent width 18 pixels) gives the spectral points some 1700 degrees of freedom and a S/N of 30. In practice, the S/N may be lower than this theoretical estimate [12].

The resulting spectrum was corrected for the stationary instrument response function. This was done by selecting a featureless image and fitting a 2-dimensional Gaussian to its smoothed SAR image modulation spectrum. The fit thus obtained was taken to be the stationary instrument response function; it is shown in Figure 2. The correction for it consists of division by this function.

The effects of speckle noise can be approximately corrected for by subtracting a constant offset from the spectrum of the speckled image [16,17]; this has effectively been done by adjusting the levels in the contour plots.

The final spectral estimate thus produced still contains no correction for the MTF (RAR nor SAR part). Hence, this procedure puts the ERS-1 derived spectra at the same status as the SHIRA spectra, which also lack absolute (wave height) calibration and MTF correction.

## 4 Results

### 4.1 In-situ hydro-meteorological data

On board the Gauss the environmental conditions were monitored. A summary is listed in Table 3. (All directions are measured clockwise from North.) Air and water temperature, wind speed and direction, and significant wave height are listed for the time of the ERS-1 and SHIRA measurements and approximately one hour earlier, in order to be able to assess variability. On date 25 the only wind measurement available was two hours before the ERS-1

overpass.

It is apparent that wind speeds during most of the experiment were high, and the waves got quite high toward the end. Date 25 shows a combination of high waves with relatively low wind speeds. On dates 19 and 20 the water was warmer than the air, leading to an unstable situation; on the other dates conditions were (nearly) neutrally stable. Conditions did not vary much during the hour before most measurements, except on date 22 when the wind turned 50°.

Wave spectra from the Datawell wave buoy at T10 have been presented before [1,2,3] and are not included anymore.

Date	Time (UT)	Water	Wave	Air	Wind	
		Temp (°C)	Height (m)	Temp (°C)	Vel (m/s)	Dir (°)
19	19:00	7.7	1.60	3.0	11	250
	20:12	7.6	1.85	2.8	11	255
	21:13	7.6	1.85	2.8	11	255
20	09:29	7.7	1.90	3.8	6	280
	10:47	7.6	1.70	4.7	7	260
22	20:15	7.7	2.80	8.0	11	180
	21:14	7.7	2.90	8.0	12	230
23	09:34	7.7	3.30	7.6	13	250
	10:50	7.7	3.10	7.2	13	250
25	19:05	8.2	4.60	7.7	3.5	140
	20:02	8.2	4.50	7.7	-	-
	21:13	8.2	4.65	7.7	-	-
28	20:19	7.9	5.30	7.0	16	210
	21:00	7.9	5.50	6.7	17	210
	21:10	7.9	5.50	6.7	17	210

Table 3: Met/ocean in-situ measurements from the Gauss. Column 4 is significant wave height.

## 4.2 SHIRA

The wave spectra as measured by SHIRA are plotted in Figure 3a-f. Each SHIRA measurement is presented as a tabloid of 12 plots. Each of the plots represents a directional wave number spectrum integrated over a limited wave frequency band as explained in section 3.1. The band width is 21 mHz and the bands are adjacent. As discussed in section 3.1, the frequency range 26 to 290 mHz is most reliable. Inspection shows that also the extreme frequencies in this range do not contain much information. Therefore, the first frequency band plotted is centered around 40 mHz and the last one around 270 mHz. So, the first image is the directional spectrum of the waves that have periods in the range 30-50 mHz; the second image is the directional spectrum of the waves that have periods in the range 51-71 mHz; etc. The band center is indicated on top, following the measurement ID.

Only the central 64×64 spectral pixels are plotted ( $k_x, k_y = -0.172$  to  $+0.172$  rad/m) because the inner (long wave) parts are the most interesting. In some cases, however, short wind waves are detected but fall outside of the plot. This effect may occur for frequencies of 205 mHz and up. Contour scaling is relative to maximum in each plot, so spectra with little energy show mostly noise contours. The axes are labeled with  $k_x$  and  $k_y$  values in units of  $10^{-2}$  rad/m. Circles of constant wavelength ( $2\pi/k$ ) are drawn for ease of reference. All spectra are rotated to North up.

Although only one SHIRA spectrum for each ERS-1 overpass is presented, all other spectra that were recorded have been processed and inspected. For most dates there are several spectra available taken around the time of ERS-1 overpass, separated by up to tens of minutes. These spectra, although not exactly identical, are quite similar. The spectra shown here are representative of all relevant SHIRA measurements, except where otherwise noted.

The six measurements will be briefly discussed.

#### Date 19

At the lowest frequencies there is almost no gravity wave energy. The longest gravity waves are about 200 m (in the 82 mHz plot). Around 100 to 120 mHz long waves of around 100 m are very clear, going over to wind waves of down to less than 50 m, all in approximately the same direction (SSE). The shortest waves are visible in the spectrum around 207 mHz. The dominant wavelength, most easily read from the integral spectrum  $F(\vec{k})$  (not shown), is 120 m, heading  $160^\circ$ .

The spectrum shown here was taken one hour before the ERS-1 overpass. Inspection of two spectra taken an hour later at 21:13 and 21:16 reveals that a new, long wave mode at 270 m,  $65^\circ$  has sprung up. These spectra are heavily affected by the motion of the platform (5 m/s) at that time; the very long waves, however, suffer the least from this effect, and the detection of this wave mode is regarded as reliable.

#### Date 20

Some very long waves appear to be present with a very large angular dispersion around 82 mHz, 270 m, heading NE. Between 120 and 230 mHz, 100 to 30 m wavelength, wind waves are detected heading SE, also with a notable directional dispersion. The dominant wavelength is 100 m, heading  $135^\circ$ .

#### Date 22

This spectrum is strongly bi-modal, with two sets of waves traveling in almost opposite directions. One component has a dominant wavelength of 190 m, heading  $45^\circ$ , the other a dominant wavelength of 130 m, heading  $190^\circ$ . The first component develops into wind waves, turning more northerly to  $0^\circ$  around 230 mHz.

#### Date 23

Very long waves of over 300 m length are seen around 60 mHz, changing over to progressively shorter waves at the higher frequencies, up to 230 mHz. The dominant wavelength is around 220 m, heading  $75^\circ$ , although the spectral peak is quite broad and might be better described by invoking an additional component at 110 m,  $30^\circ$ . The wind waves (190 mHz and up) are mainly around  $90^\circ$ .

#### Date 25

This is an apparently simple situation with the propagation direction for all wavelengths around  $35^\circ$ . However, during this measurement the Gauss was sailing at a speed of 3 knots. The effect is noticed through an apparently higher frequency for the gravity waves, which is equivalent to a longer wavelength given the frequency. As a result, however, the spectra at the higher frequencies are not easily interpreted anymore; they may be dominated by aliasing. The dominant wavelength is 210 m.

### Date 28

Here the wave field is uni-modal with a direction of  $50^\circ$ . Longest waves detected are over 300 m, dominant wavelength is 230 m. Short waves around and below 50 m may be seen in the spectra around 186 and 207 mHz, turning over to a somewhat more easterly direction.

### 4.3 ERS-1 SAR

The six directional wave spectra from the ERS-1 SAR obtained as described in section 3.2 are presented in Figure 4a-f. These spectra show a  $180^\circ$  ambiguity as the wave propagation direction is not resolved. The azimuth direction (Table 1) is indicated in the plots.

The spectra represent the ocean wave spectrum averaged over 90 km squared, almost the entire ERS-1 scene. The individual spectra of  $1024^2$  pixels (12.8 km squared) that make up the average have been separately inspected. There were differences between the individual spectra, also in a systematic way as a function of position, but these differences were always small, indicating a fair degree of homogeneity over the 90 km area.

All spectra show some excess energy at the high wave numbers in range direction, indicating that the stationary instrumental spectral response function was somewhat underestimated there. Our estimate of the response function is probably not very good; it was based on the spectrum of the date 19 image with the spectral peaks removed. This image was the most homogeneous one available to us.

The ERS-1 spectra show the characteristics typical of SAR spectra. The SAR ocean wave imaging mechanism is dominated by the velocity bunching effect [10,18,19], which causes a distortion in the spectra. The distortion is particularly severe when the imaging becomes strongly non-linear. This occurs for values  $> \sim 1$  of the non-linearity parameter [20,21]

$$C = (R/V)g^{1/2}k_d^{3/2}G|\cos\phi_a|(H_s/4) = 1200\lambda_d^{-3/2}|\cos\phi_a|H_s, \quad (3)$$

where  $k_d$  and  $\lambda_d$  are k-number and wavelength of the dominant wave,  $\phi_a$  its direction of propagation w.r.t. azimuth,  $G$  a geometrical factor which is close to 1 for ERS-1, and  $H_s$  the significant wave height. The numerical values for the ERS-1 have been substituted using Table 2.

Taking the dominant wavelength and direction from the SHIRA data and the significant wave height from Table 3, values for  $C$  between 0.6 and 2.1 are found; this means that in all cases the imaging is non-linear [10]. One consequence is that the spectra cannot be inverted in a simple way anymore, but only through iterative techniques [21,22], which is beyond the scope of the present report. However, the most significant improvement to linear modeling is the quasi-linear form, in which the linear transformation is modified by a Gaussian azimuth cutoff factor  $\exp(-(1/2)(k_a/k_\sigma)^2)$ , with  $k_a$  the wave number in azimuth direction [11,13,14]. The cutoff occurs at

$$\lambda_\sigma = 2\pi/k_\sigma = K(R/V)H_s, \quad (4)$$

with proposed values for  $K$  of e.g. 3.93 [11] or 1.1 [13,14]. This azimuth cutoff is clearly present in all spectra; no correction has been made for it.

In the following the six ERS-1 measurements will be briefly discussed and compared to the SHIRA results.

### Date 19

The main feature in this spectrum is a peak at 300 m, heading  $60^\circ$ . This corresponds to the long wave mode found in the SHIRA spectra of 21:13 and 21:16 which were not yet present at the time the SHIRA measurement of Figure 3a was made. The SHIRA waves of 150 m and less with a SSW heading are not found in the ERS-1 spectrum; they seem to be suppressed by the azimuth cutoff, which also creates the tilted band across the spectrum. The value of the non-linearity parameter  $C$  is 1.7, based on the SHIRA data and the significant wave height, so the imaging is strongly non-linear.

**Date 20**

Here, both sets of waves seen in the SHIRA spectra are present: the long waves heading NE, and the shorter waves heading SW. In both cases, the heading is biased towards the range axis, which may be expected [20,21]. The non-linearity parameter is 1.0.

**Date 22**

This is a uni-modal spectrum with a peak at 200 m, 60°. This reflects the wave component with NE heading from the SHIRA spectra; the wave component with southerly heading is not found anymore. When the non-linearity parameter is calculated separately for the first (NE) and the second (S) component, values of 0.6 and 2.1 are found.

**Date 23**

A broad peak is seen, centered around 170 m, 85°, in accordance with the SHIRA result.  $C$  is only 0.7 here.

**Date 25**

The peak around 250 m, 50° reflects the SHIRA dominant wavelength of 210 m, 35°.  $C$  is 1.2.

**Date 28**

The spectrum with a single peak at 280 m, 65° is a fair representation of the SHIRA spectrum, where waves up to 300 m propagate in the 50° direction. The  $C$  value is not very high at 0.8.

**Summary**

The SHIRA/ERS-1 comparison is summarized in Table 4. In that table the wavelength and direction  $\lambda_p, \phi_p$  of the maxima in the spectra are listed, whereas in the preceding discussion the centers of gravity of the spectral peaks were quoted, as estimated by eye from the plots. These numbers can be different, especially for the detailed SHIRA spectra. Of course, the spectra are not characterized at all well by these few numbers.

The table also contains  $\tilde{\phi}_a$ , which is  $\phi_a$ , the wave propagation direction w.r.t. the ERS-1 flight direction, reduced to the interval  $[0^\circ, 90^\circ]$ ; azimuth traveling waves have  $\tilde{\phi}_a=0^\circ$ , range traveling waves have  $\tilde{\phi}_a=90^\circ$ .  $\tilde{\phi}_a$  was calculated using SHIRA's  $\phi_p$ .

## 5 Discussion

### 5.1 Results of the intercomparison

In evaluating the intercomparison between the SHIRA and ERS-1 spectra made in the previous section, the following points have to be kept in mind.

First, as can be seen from Table 2, the images of the ERS-1 SAR are on a much larger scale than SHIRA's. Both the resolution of the ERS-1 and the image size are larger than those of SHIRA. Nevertheless, the homogeneous conditions expected (and found, ref. section 4.3) in the Norwegian Sea make the comparison meaningful, although the scale and location differences can be expected to cause some degree of disparity.

Secondly, the ERS-1 spectra were not corrected for any velocity bunching MTF, and neither type of spectrum was corrected for any RAR MTF (the real aperture radar modulation transfer function, which is applicable to both sensors); the RAR MTFs of the two sensors will not be identical, however, due to the differences in incidence angle, polarization, and frequency.

Date	SHIRA		ERS-1		$\tilde{\phi}_a$	$C$	$\lambda_\sigma$
	$\lambda_p$	$\phi_p$	$\lambda_p$	$\phi_p$			
19	270 m	065°	320 m	060°	80°	0.1	210 m
	120 m	165°	-	-	00°	1.7	210 m
20	300 m	060°	270 m	065°	45°	0.3	190 m
	090 m	120°	090 m	115°	75°	1.0	190 m
22	190 m	055°	190 m	060°	70°	0.6	320 m
	130 m	190°	-	-	25°	2.1	320 m
23	220 m	080°	190 m	085°	65°	0.7	340 m
	110 m	035°	-	-	20°	3.1	340 m
25	210 m	030°	240 m	050°	45°	1.2	520 m
28	260 m	060°	280 m	060°	75°	0.8	610 m

Table 4: Wavelength and direction of the peaks in the SHIRA and ERS-1 spectra, wave direction w.r.t. ERS-1 azimuth  $\tilde{\phi}_a$ , the non-linearity parameter  $C$ , and the expected azimuth cutoff wavelength  $\lambda_\sigma$  (using  $K=1.1$ ).

Thirdly, the SHIRA spectra are believed to be a reasonably good representation of the true wave height spectra, based on comparisons with buoy measurements (e.g. [3,4]). However, the need to measure very long waves and the consequent undersampling in this experiment may have created some aliasing contributions from the shorter waves.

Taking these points into account, the ERS-1 spectra as compared to the SHIRA spectra are seen to possess the characteristics expected for SARs with relatively high  $R/V$  ratios: they are dominated by an azimuth cutoff  $\lambda_\sigma$ , range traveling and longer waves are better imaged, spectral peaks shift towards the range axis, and imaging is suppressed or severely distorted for wave modes with larger values of the non-linearity parameter  $C$ . The shorter waves ( $\lambda < 75$  m) that are present in the SHIRA spectra are almost never detected by ERS-1. In contrast, SHIRA is able to detect all wave components that are seen by ERS-1.

It is obvious that the ERS-1 is capable of imaging ocean waves, but the results have to be interpreted carefully using knowledge of the SAR imaging mechanism. The accuracy of the final, geophysical product, a calibrated wave height spectrum, will depend critically on the assumptions made in the SAR imaging model. SHIRA, on the other hand, gives a more direct look at the wave spectrum on account of its much simpler imaging mechanism. In part due to its higher resolution, it is able to image much shorter waves than ERS-1 can, whereas only some very long waves may be more easily detected by ERS-1 because of its much larger field of view.

## 5.2 Future work

The present analysis can be improved and extended on the following points, which were not within the scope of the present project.

The quality of the SHIRA spectra can be enhanced by using a gravity wave filter (only passing energy on the dispersion relation), and by averaging several consecutive spectra to raise the S/N ratio.

Correction for the RAR MTF should be applied to both sensors, but first the SHIRA MTF in particular should be established well enough.

The ERS-1 spectra can be inverted, correcting for a linear velocity bunching MTF, or better using iterative techniques.

A more homogeneous ERS-1 image than the one used now should be used to derive the stationary instrumental response function, and the same type of procedure should be used on the SHIRA data.

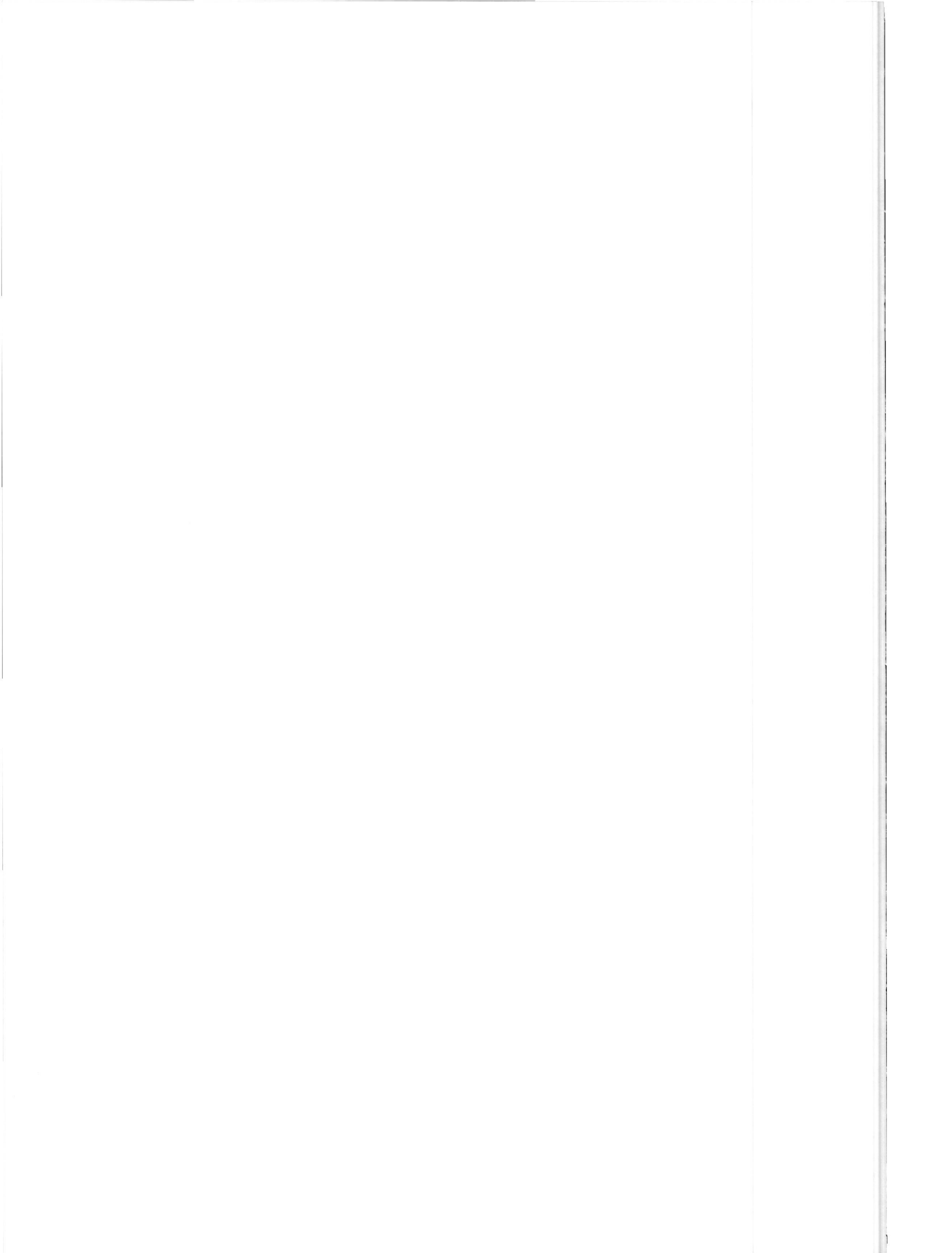
Co-location of the measurements can be improved upon by using data from different

ERS-1 scenes (ref. Figure 1) and averaging over a smaller spatial extent.

The data set available at TNO FEL and ESA obtained from the RENE 91 campaign is quite unique, and valuable enough to warrant future work along these lines. The results can play a role in the assessment of the geophysical reliability of present and future ocean wave remote sensing applications.

#### **Acknowledgement**

This report is partly based on data from the ERS-1 satellite of ESA. All ERS-1 data are copyright ESA 1991, 1994. The use of the Gauss as a platform for SHIRA is greatly appreciated.



## References

- [1] J.C.M. Kleijweg, D. Schrader, 1992, "Validation of wavenumber spectra from ERS-1 with Dutch airborne and ground based radar data obtained in RENE 91", proc. ERS-1 geophysical validation workshop, Penhors 27-30 April 1992, ESA WPP-36, p. 41
- [2] J.C.M. Kleijweg, H. Greidanus, 1993, "Validation of directional wave spectra from the ERS-1 during the ESA cal/val campaign", proc. First ERS-1 symp., Cannes 4-6 November 1992, ESA SP-359, Vol. 1, p. 31
- [3] J.C.M. Kleijweg, H. Greidanus, 1992, "ERS-1 directional wave spectra validation with the airborne SAR 'PHARS'", BCRS report 92-18, ISBN 90-5411-061-9 (also FEL report 92-C282)
- [4] J.C.M. Kleijweg, 1991, "SHIRA systeembeschrijving en eerste meetresultaten", FEL report 91-B103 (in Dutch)
- [5] H. Greidanus, J.C.M. Kleijweg, 1993, "SHIRA: a mobile radar system for measuring ocean waves, currents and slicks", proc. symp. Operationalization of remote sensing, Enschede 19-23 April 1993, Vol. 3, p. 223
- [6] L. Proud, B. Battryck (eds.), 1992, "ERS-1 user handbook", ESA SP-1148, ISBN 92-9092-029-7
- [7] P. Vass, B. Battryck (eds.), 1992, "ESA ERS-1 product specification" Issue 3.0, ESA SP-1149, ISBN 92-9092-033-5
- [8] O.M. Phillips, 1977, "The dynamics of the upper ocean" 2nd edition, Cambridge University Press, ISBN 0-521-29801-6
- [9] W.C. Keller, J.W. Wright, 1975, *Radio Sc.* **10**, 139
- [10] W.R. Alpers, D.B. Ross, C.L. Rufenach, 1981, *J. Geophys. Res.* **86** (C7), 6481
- [11] F.M. Monaldo, D.R. Lyzenga, 1986, *IEEE Tr. Geosci. Remote Sensing* **GE-24** (4), 543
- [12] F. Monaldo, 1991, *IEEE Tr. Geosci. Remote Sensing* **29** (1), 113
- [13] K. Hasselmann, S. Hasselmann, C. Brüning, A. Speidel, 1991, in R.C. Beal (ed.), "Directional ocean wave spectra", Johns Hopkins University Press, London, ISBN 0-8018-4261-1, p. 117
- [14] D.G. Tilley, 1991, in R.C. Beal (ed.), "Directional ocean wave spectra", Johns Hopkins University Press, London, ISBN 0-8018-4261-1, p. 110
- [15] P.W. Vachon, A.S. Bhogal, N.G. Freeman, 1991, in R.C. Beal (ed.), "Directional ocean wave spectra", Johns Hopkins University Press, London, ISBN 0-8018-4261-1, p. 104
- [16] A.D. Goldfinger, 1982, *IEEE Tr. Aerosp. Electron. Syst.* **AES-18** (5), 675
- [17] W. Alpers, K. Hasselmann, 1982, *Int. J. Remote Sensing* **3** (4), 423
- [18] M.J. Tucker, 1985, *Int. J. Remote Sensing* **6** (7), 1059
- [19] K. Hasselmann, R.K. Raney, W.J. Plant, et al., 1985, *J. Geophys. Res.* **90**, 4659
- [20] W. Alpers, 1983, *J. Geophys. Res.* **88** (C3), 1745
- [21] C. Brüning, W. Alpers, K. Hasselmann, 1990, *Int. J. Remote Sensing* **11** (10), 1695
- [22] K. Hasselmann, S. Hasselmann, 1991, *J. Geophys. Res.* **96** (C6), 10713



## Figures

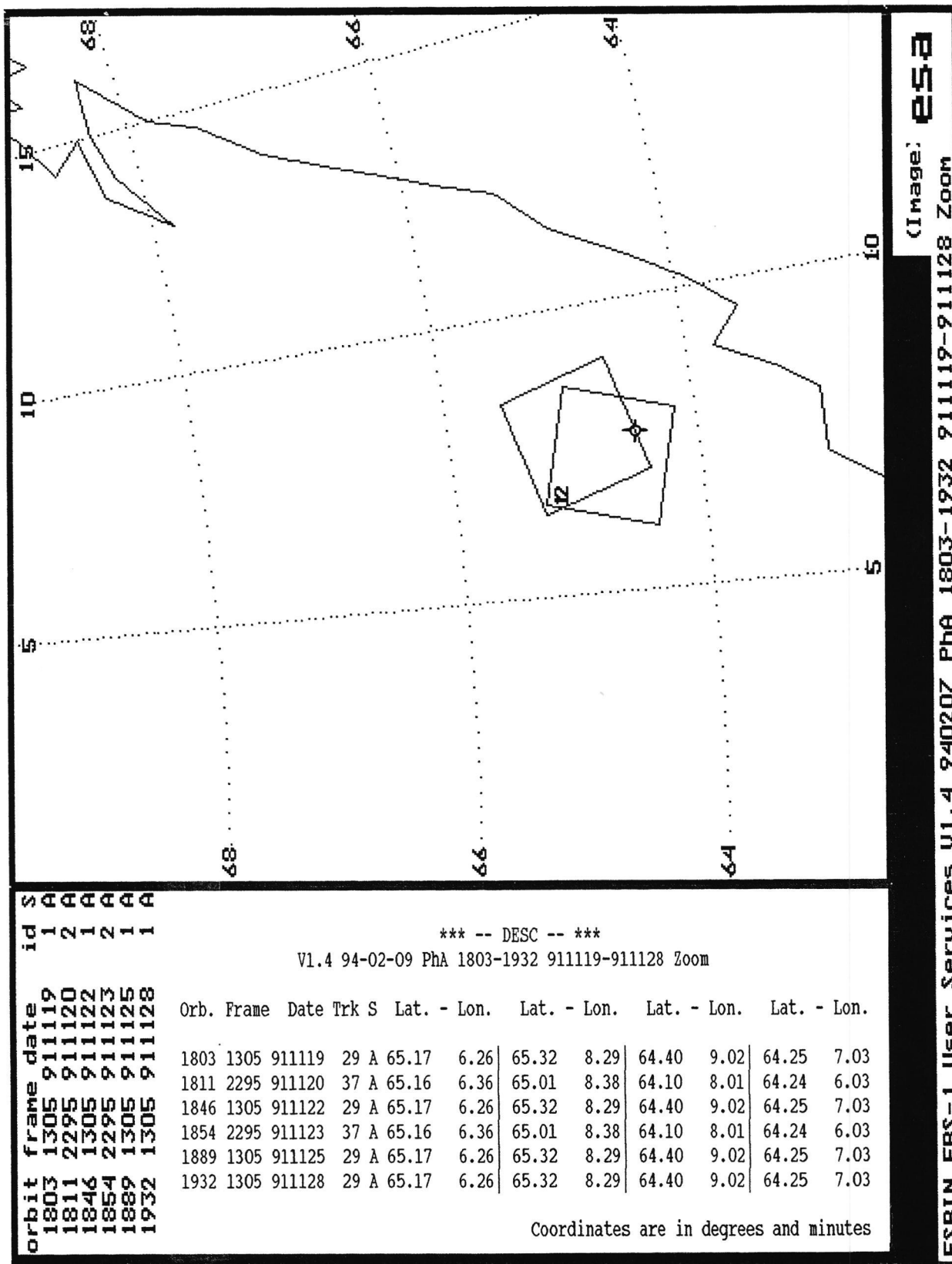


Figure 1. The locations of the ERS-1 SAR scenes. The position ("T10") of SHIRA and the Datawell buoy is indicated. The coastline of Norway is drawn. This plot is output from ESRIN's "DESC" program.

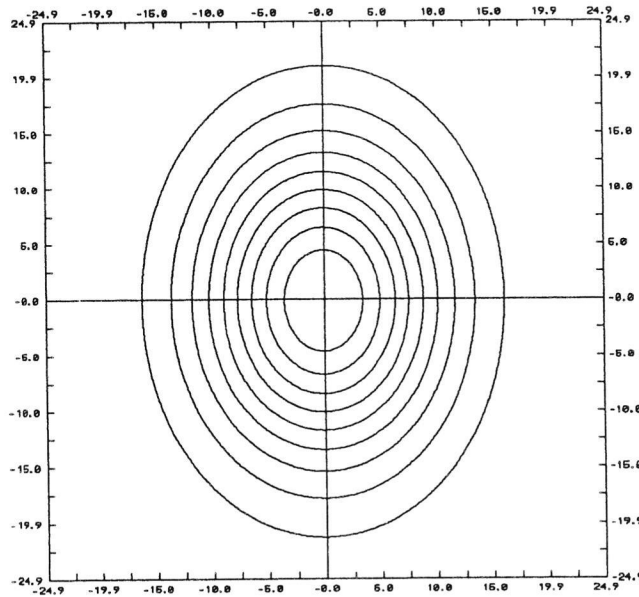
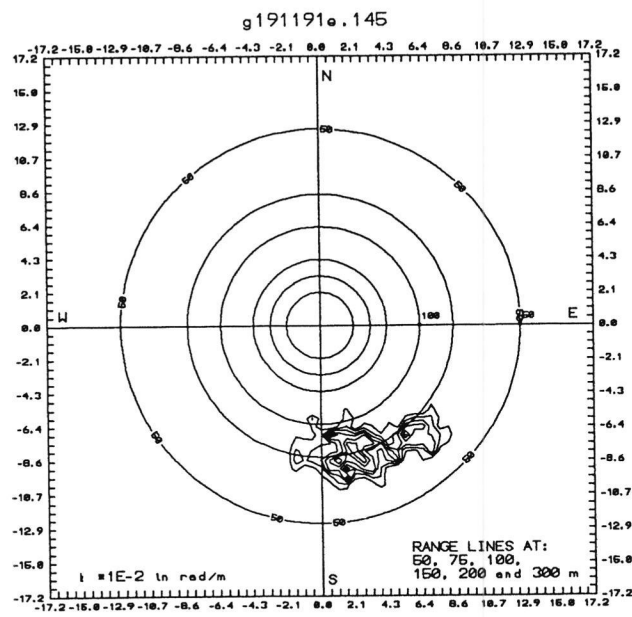
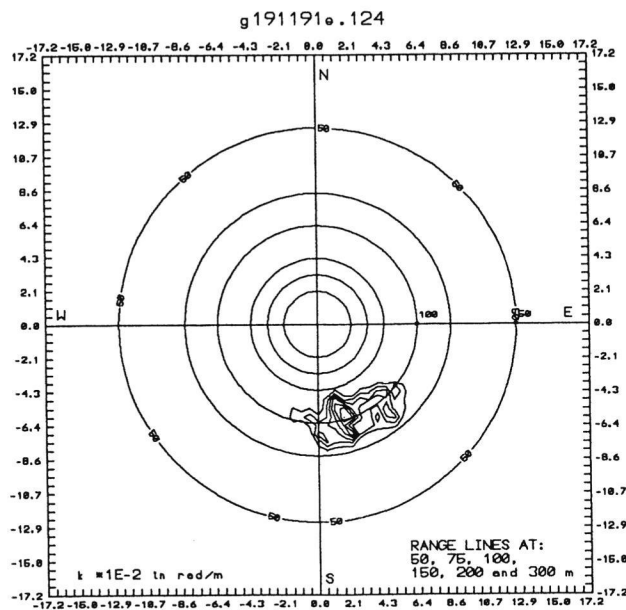
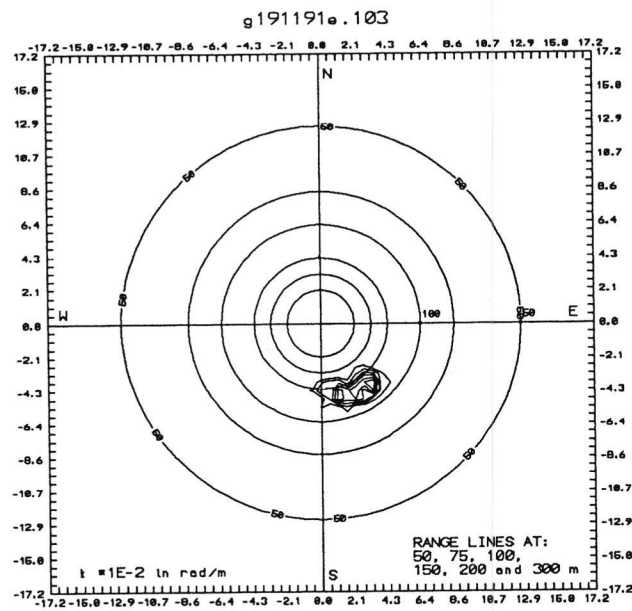
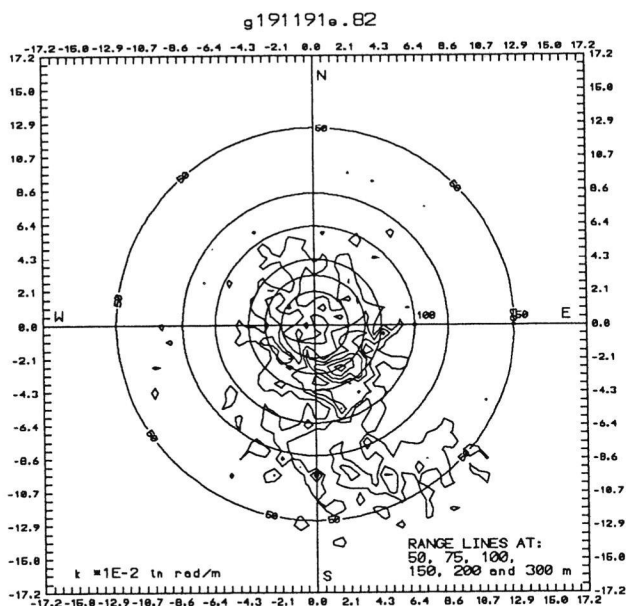
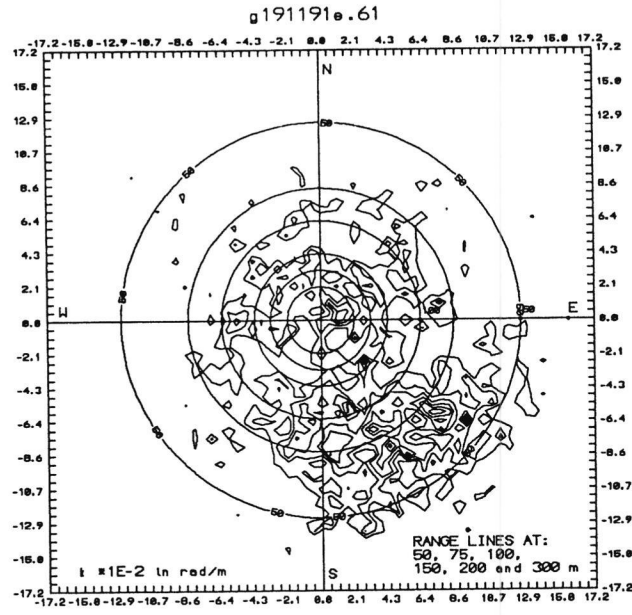
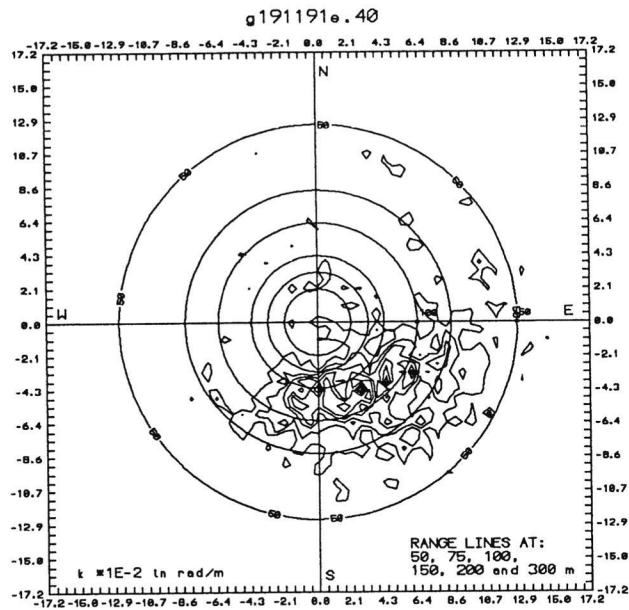
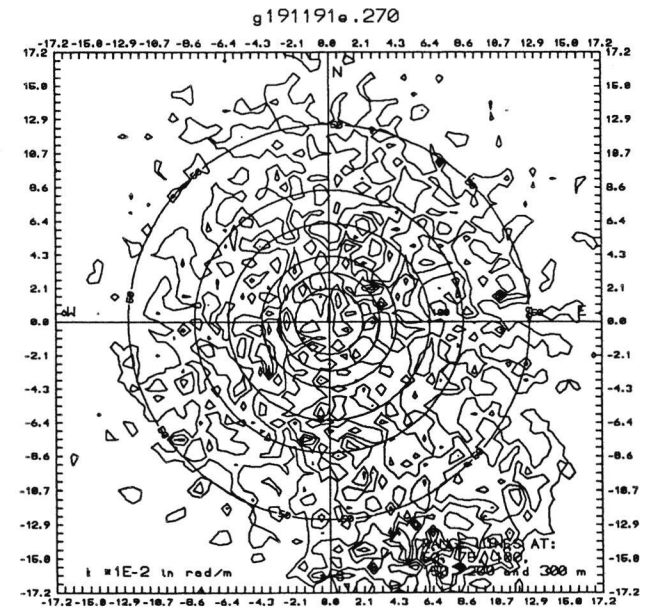
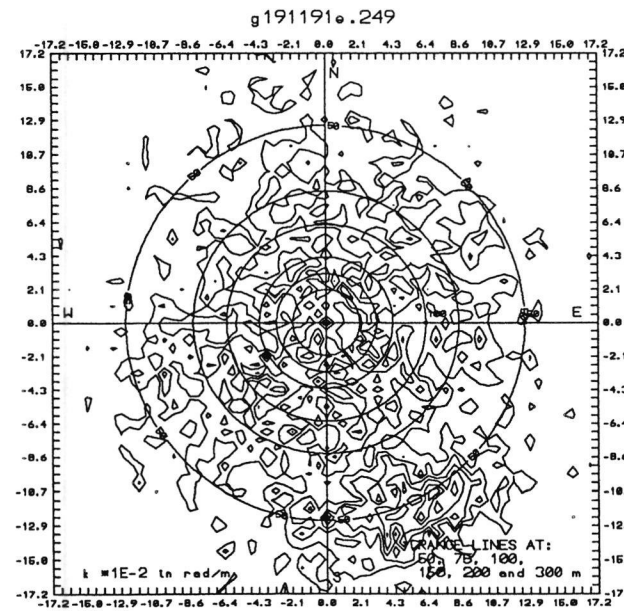
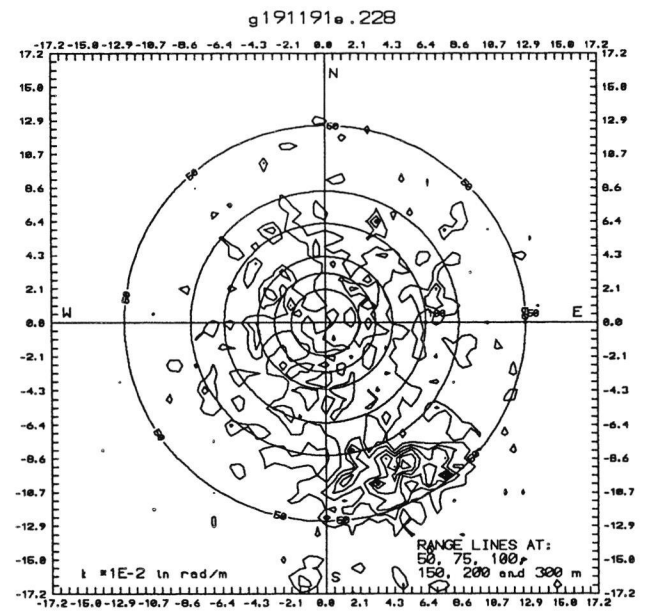
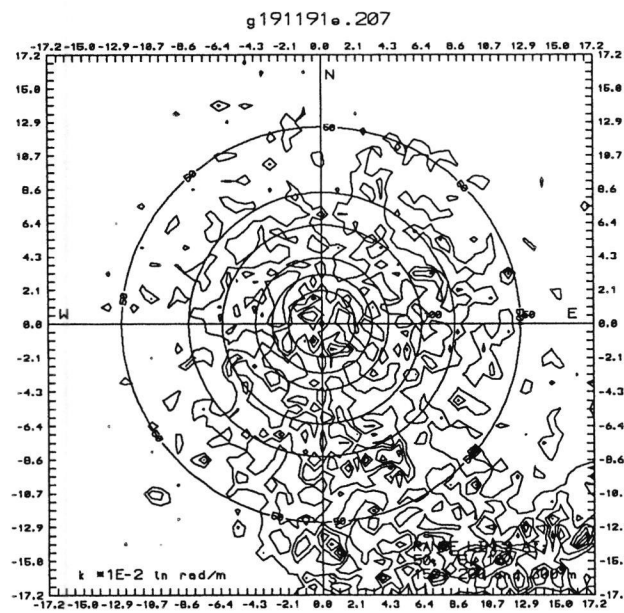
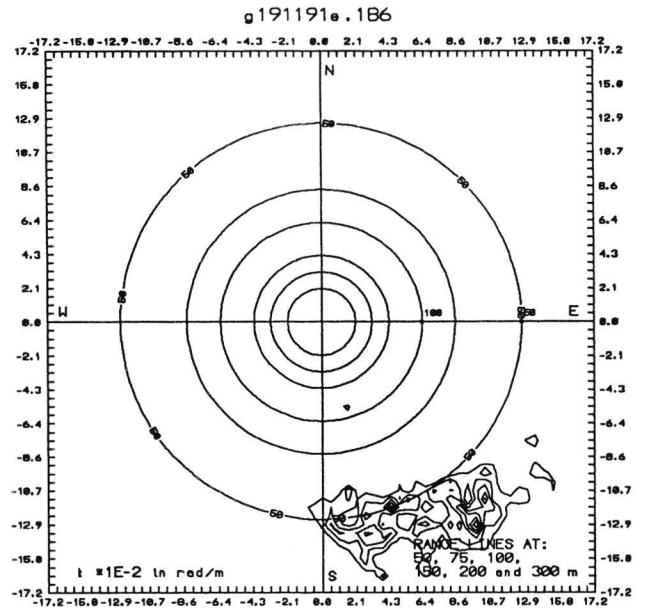
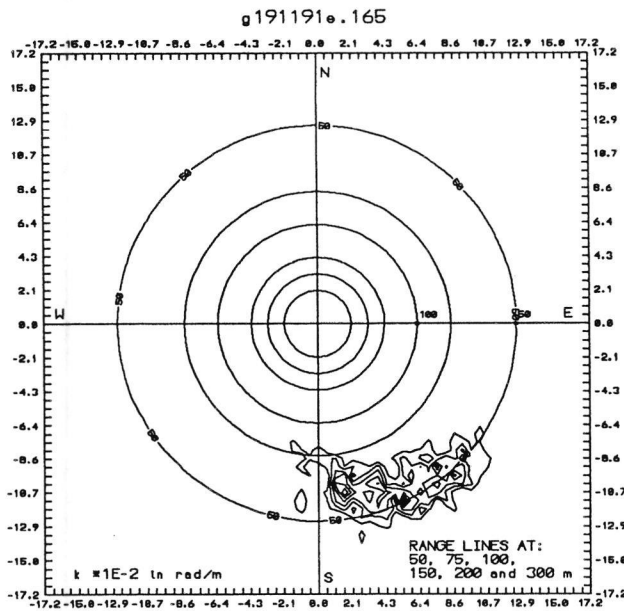
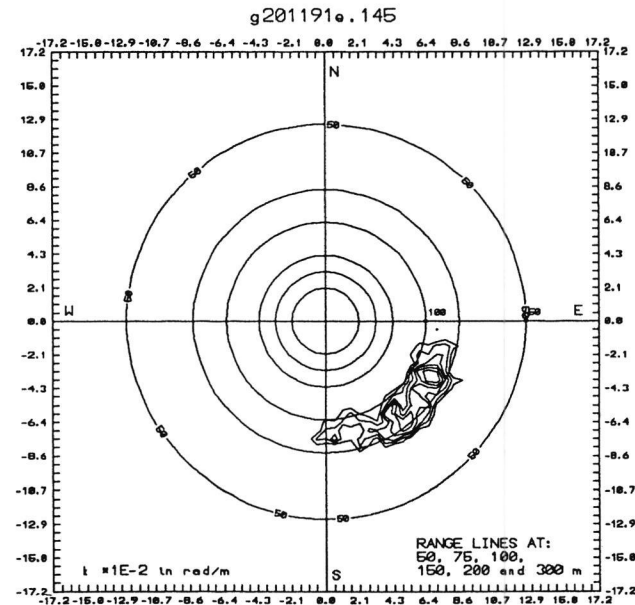
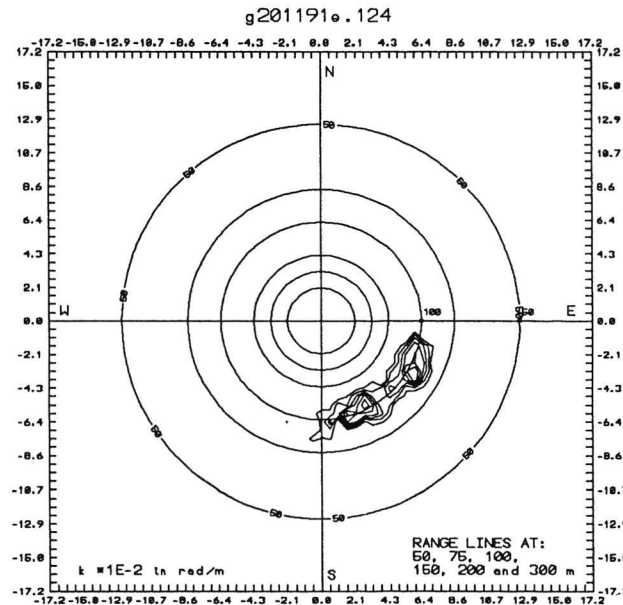
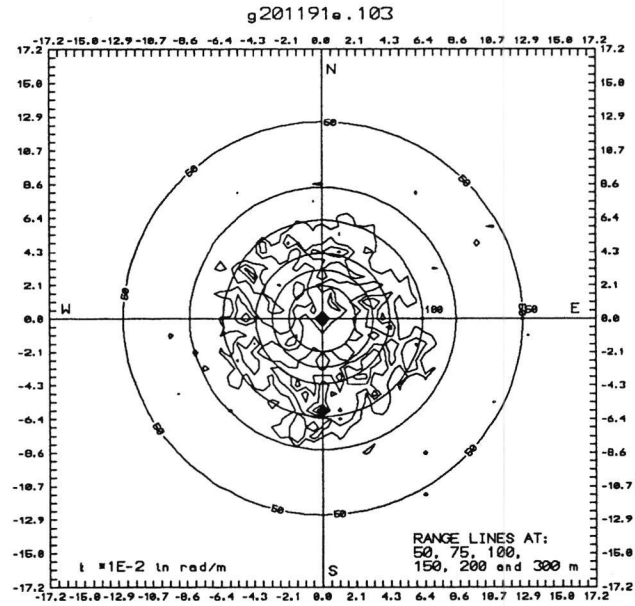
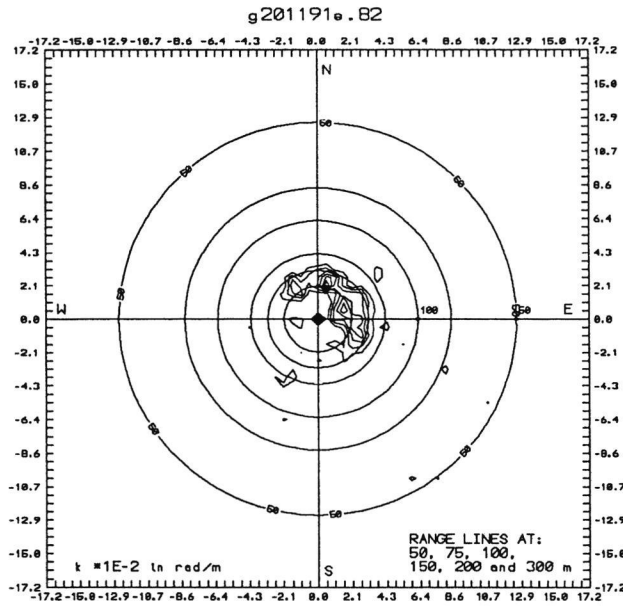
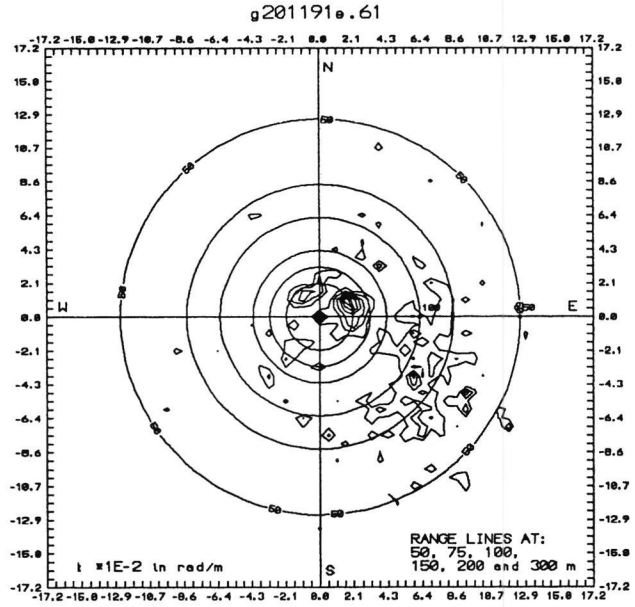
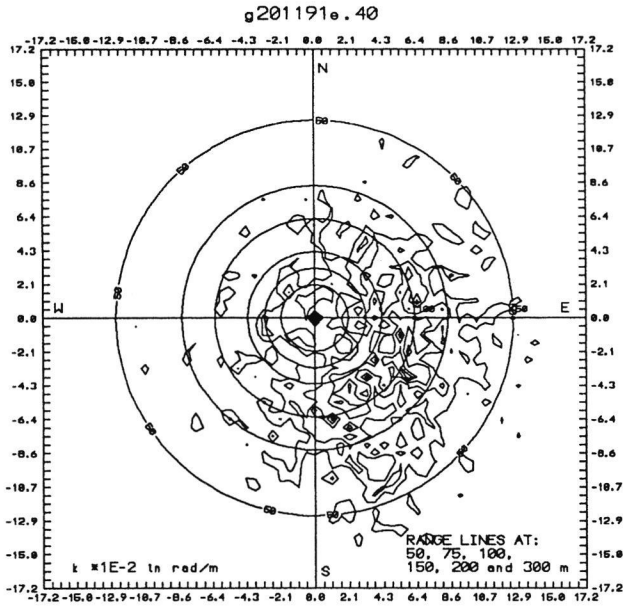


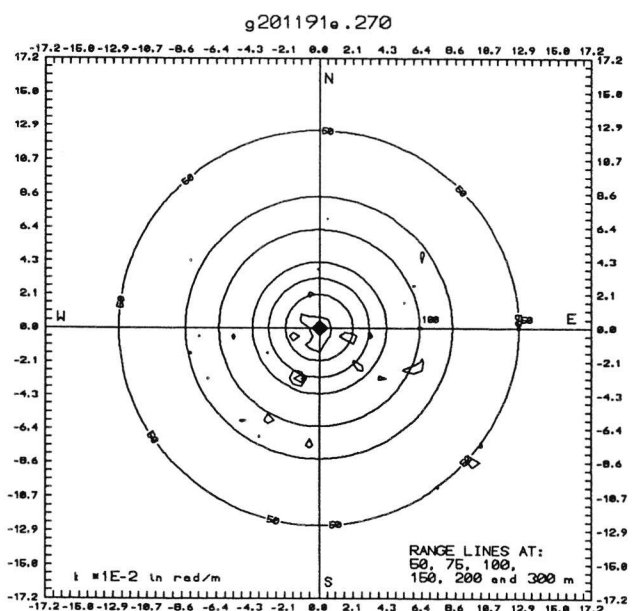
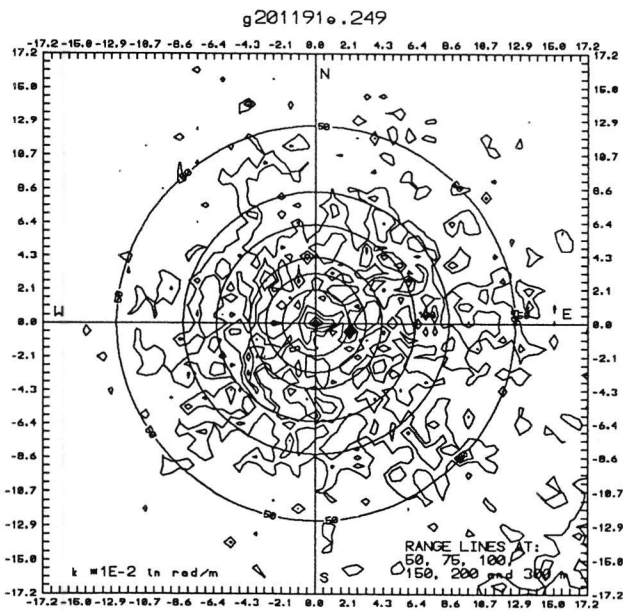
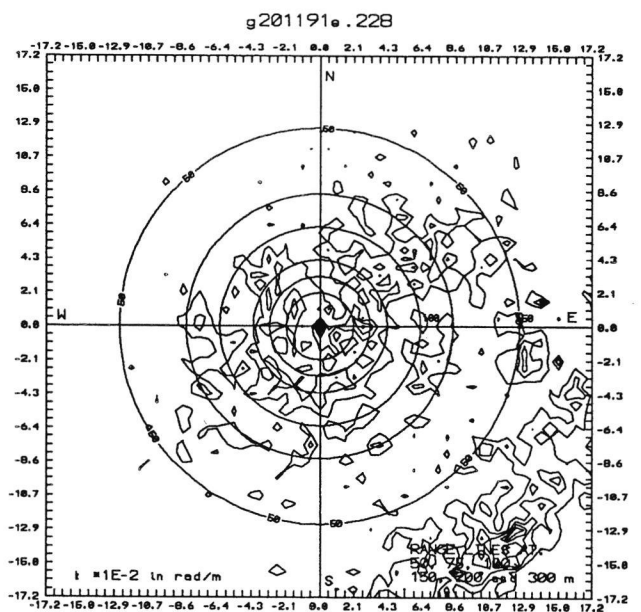
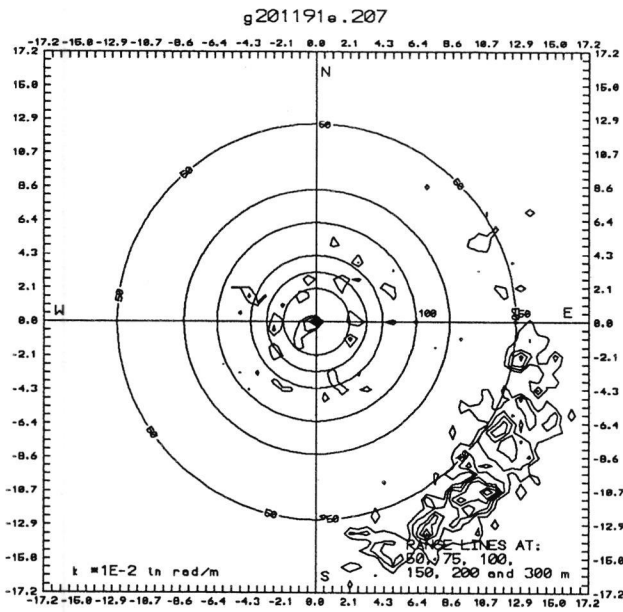
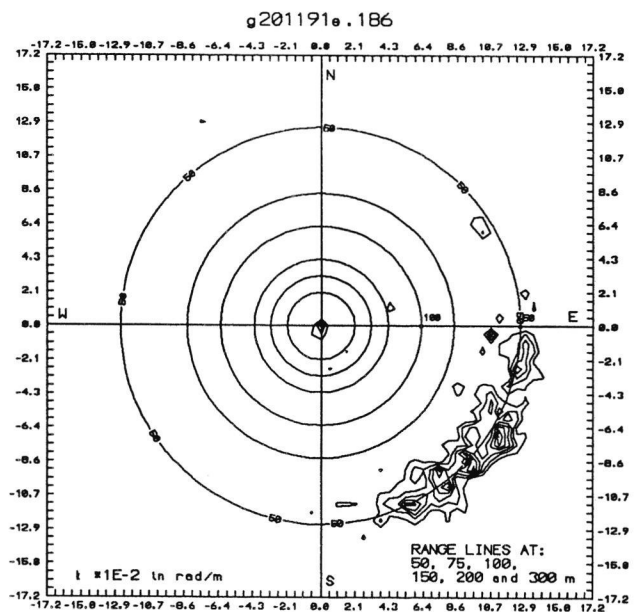
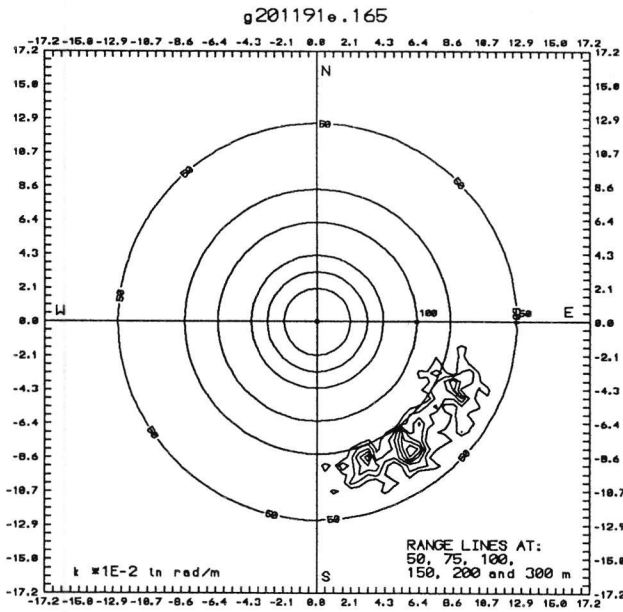
Figure 2. ERS-1 spectral stationary instrumental response function. Range direction wave number is horizontal, azimuth vertical. Axes are labeled in units of  $10^{-2}$  rad/m; contours are at 10, 20, ..., 90% of maximum.

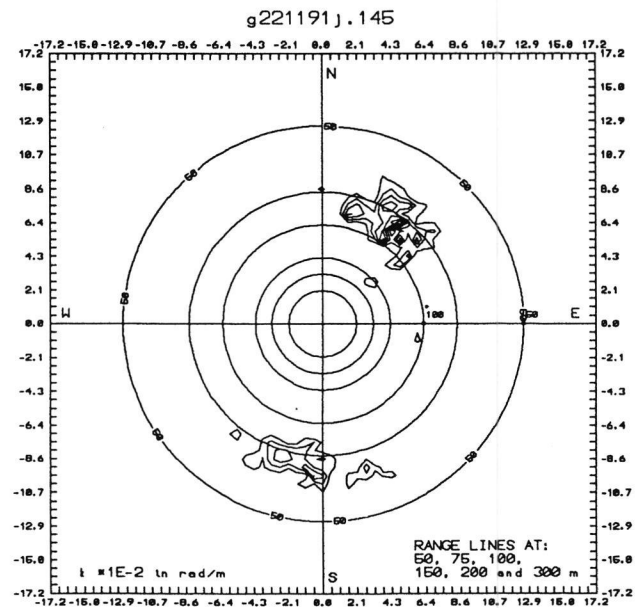
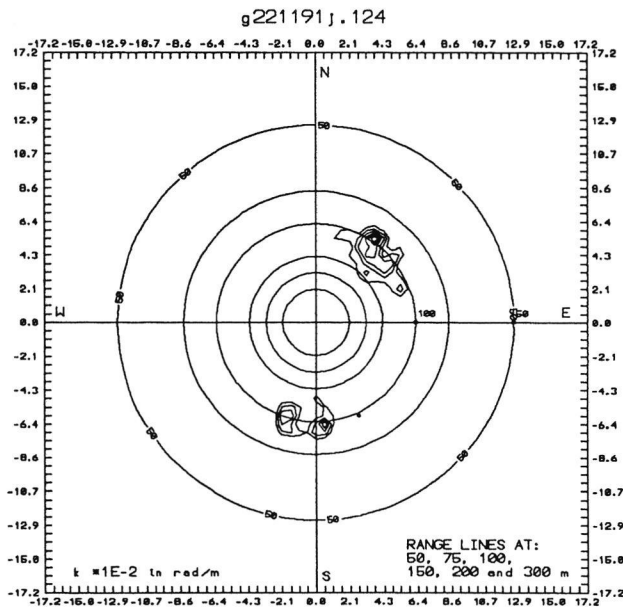
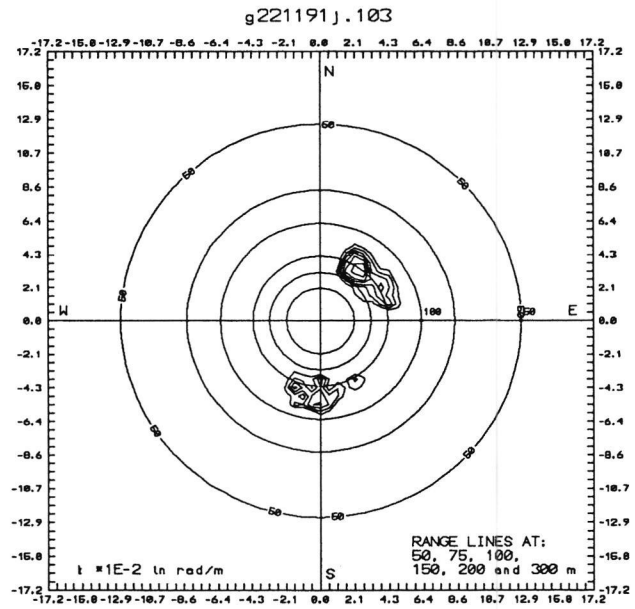
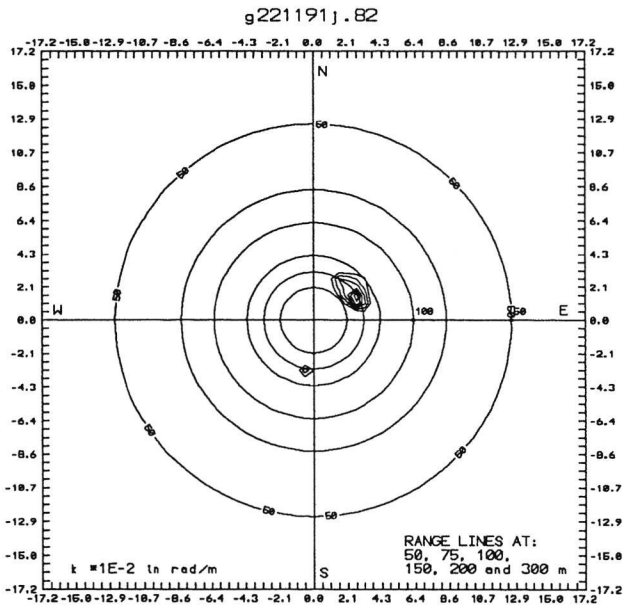
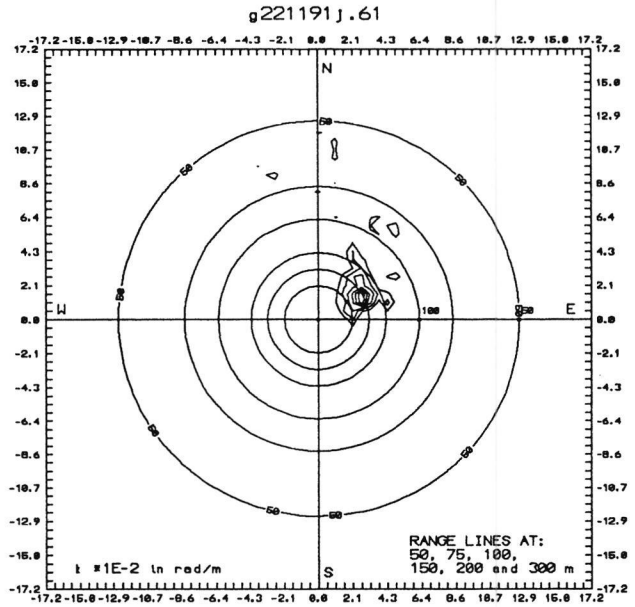
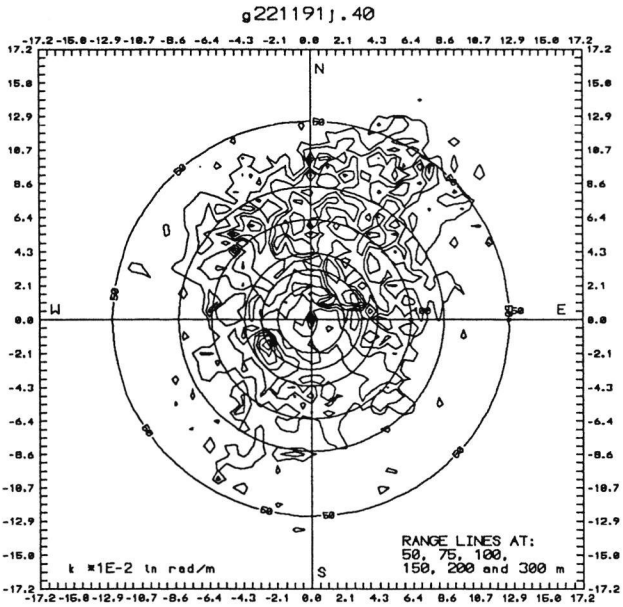
Figure 3 a-f (on the following pages, 22-33). SHIRA directional wave spectra subdivided into adjacent frequency bands. The band center is indicated in mHZ on top of each plot, following the measurement ID. Twelve plots constitute one measurement. Contours are spaced relative to the maximum in each plot. For a full explanation and legend see section 4.2.

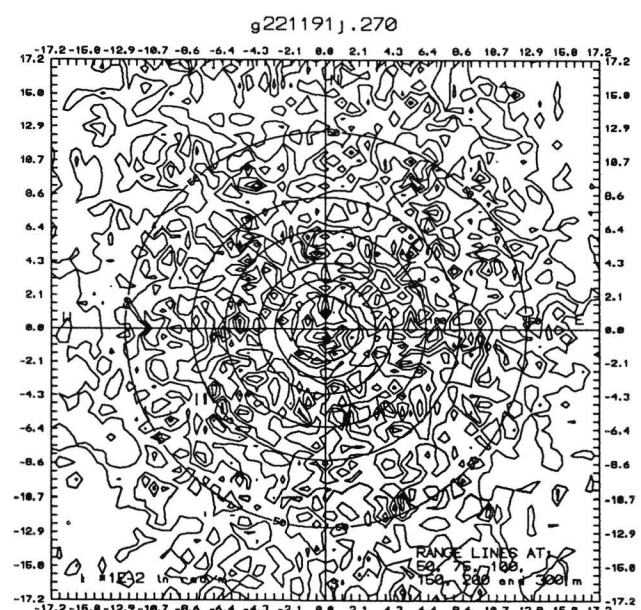
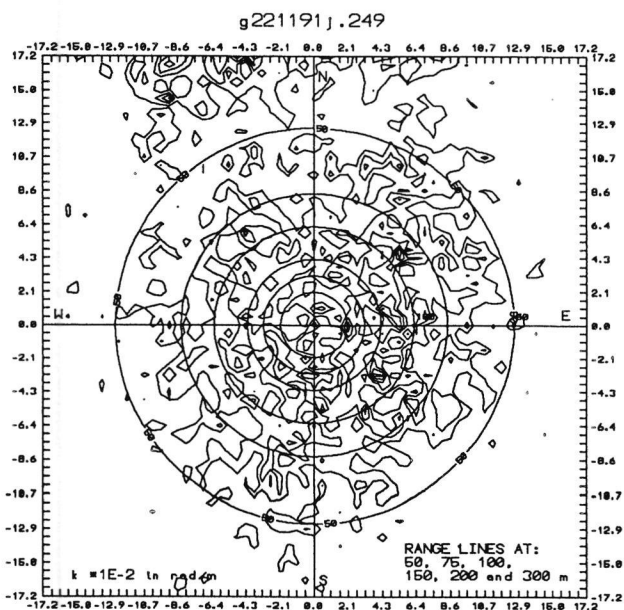
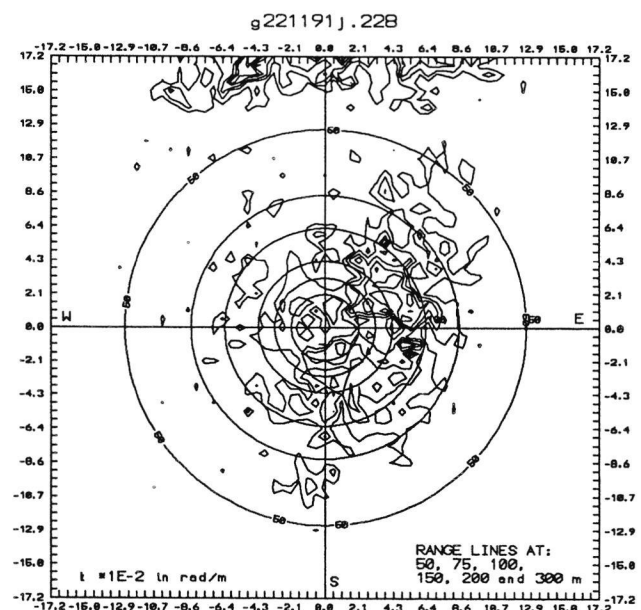
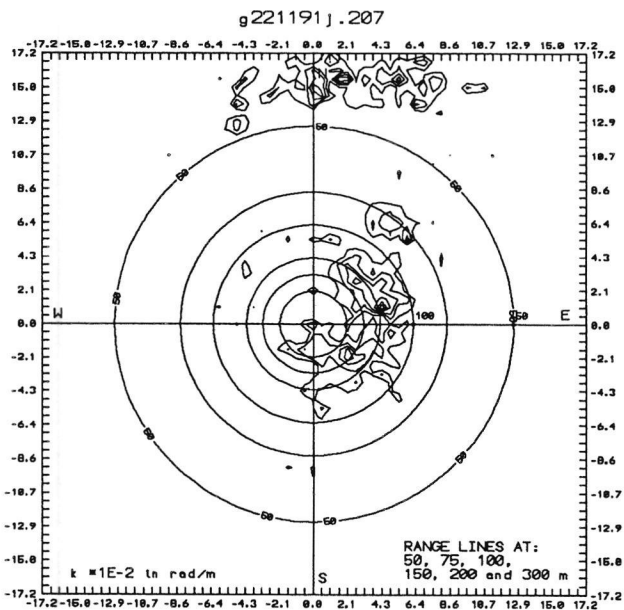
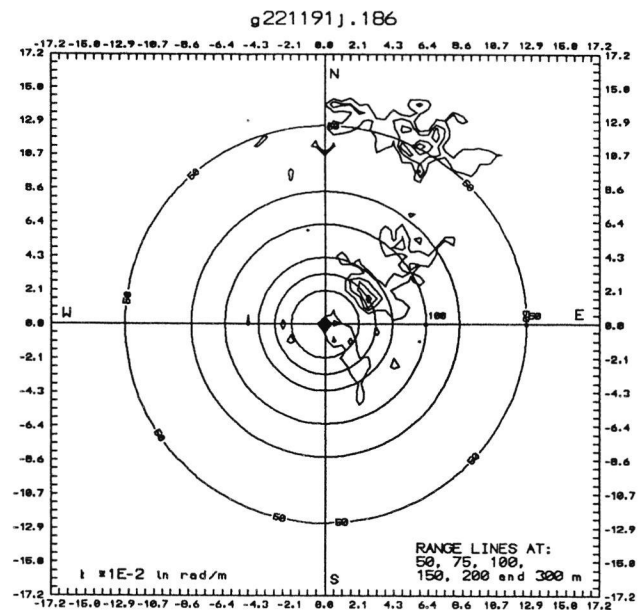
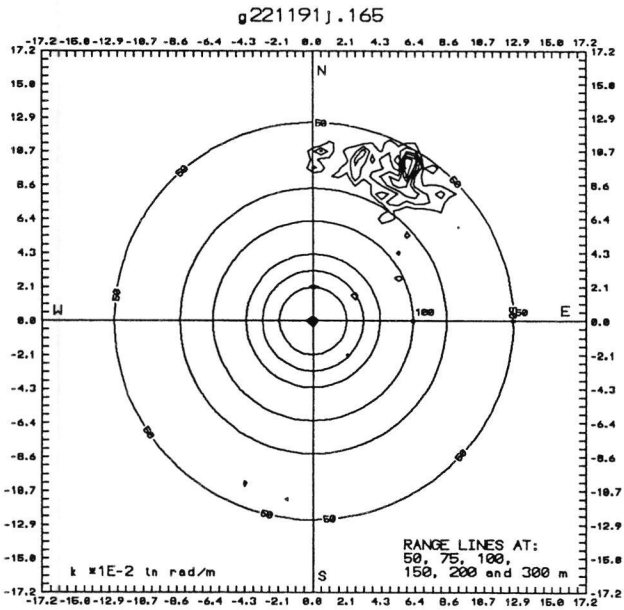


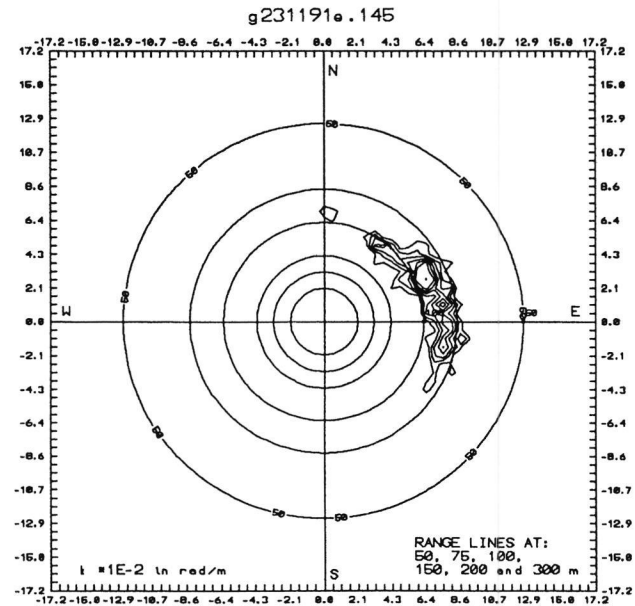
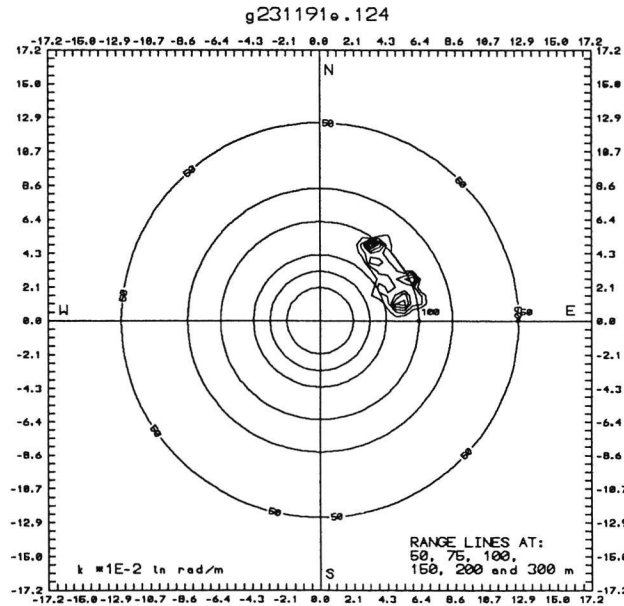
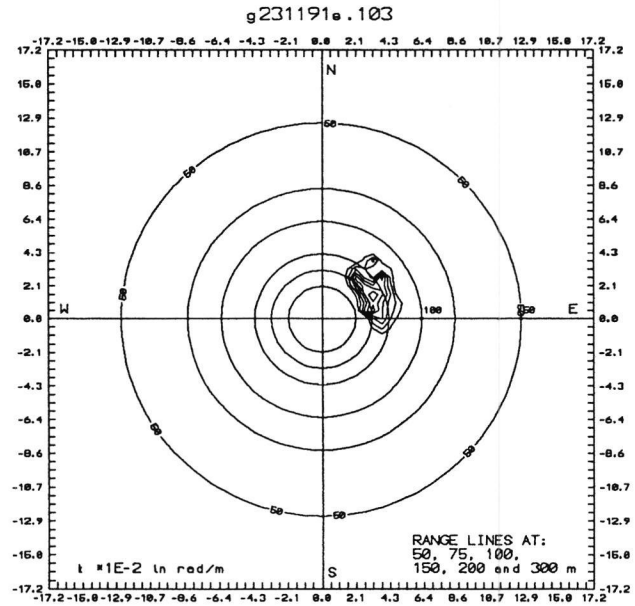
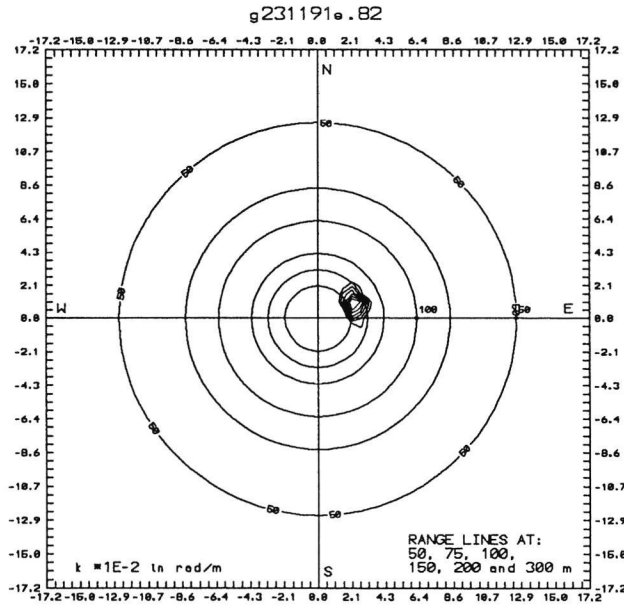
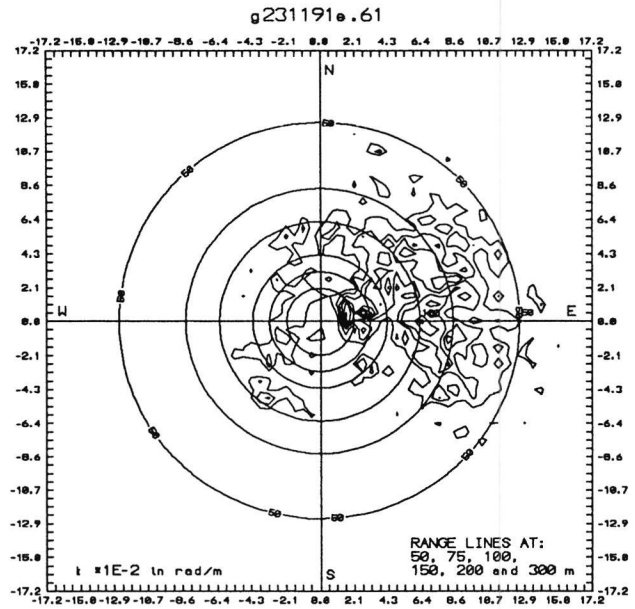
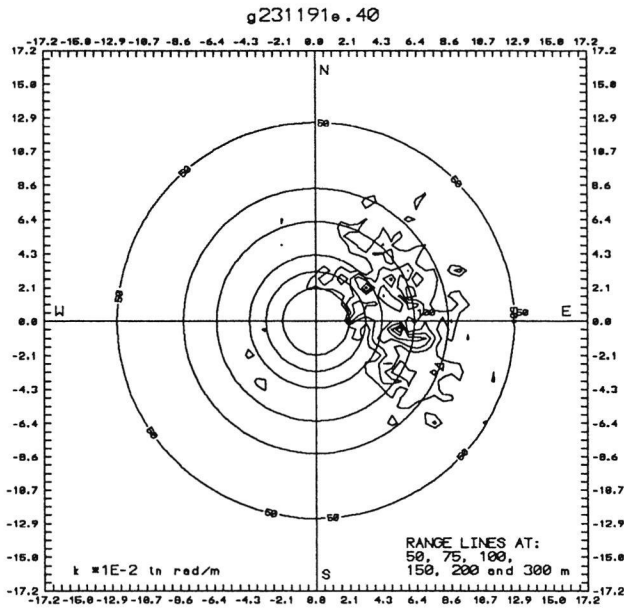


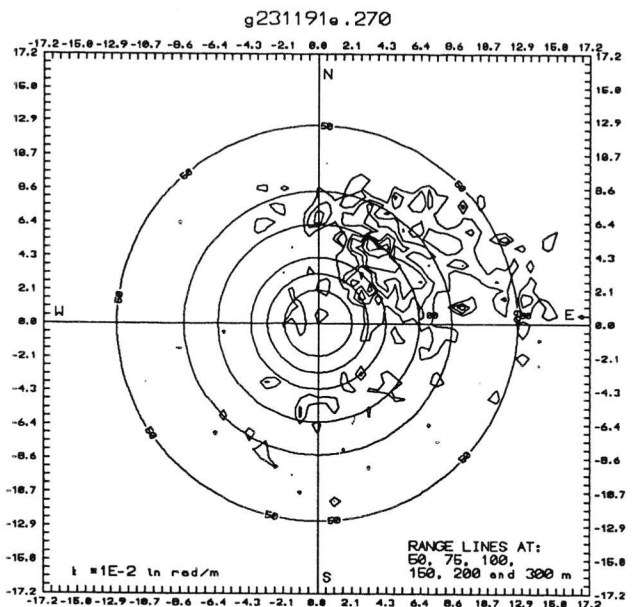
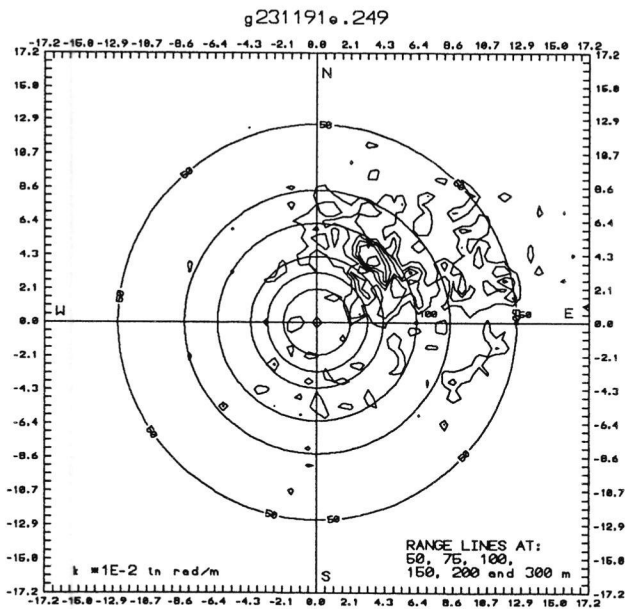
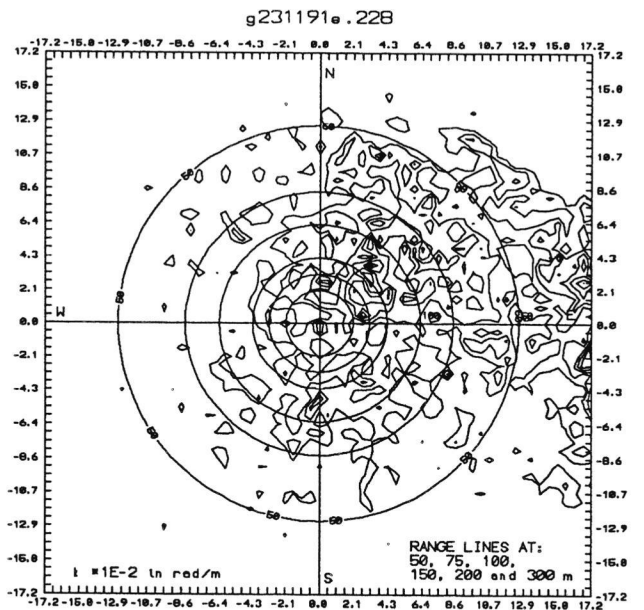
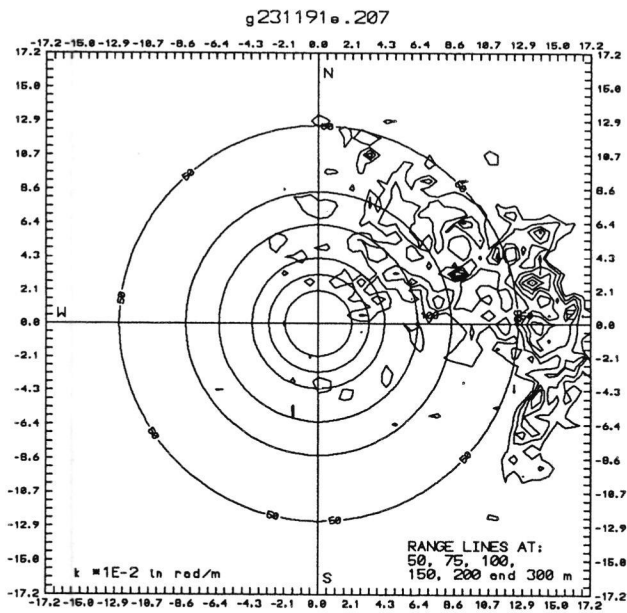
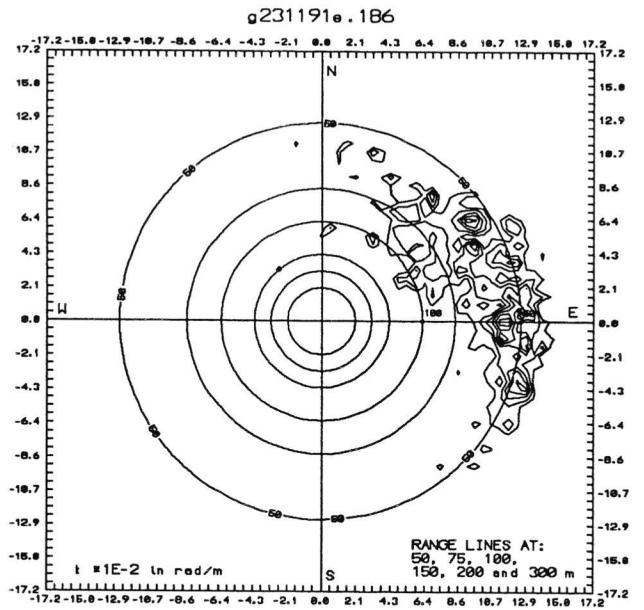
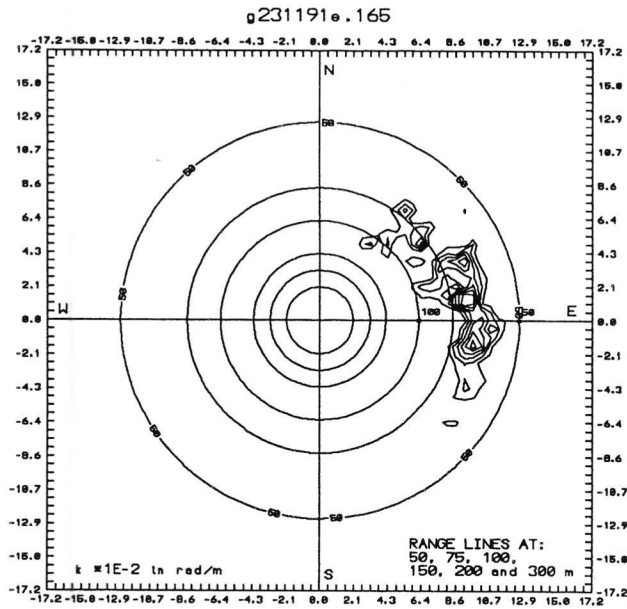


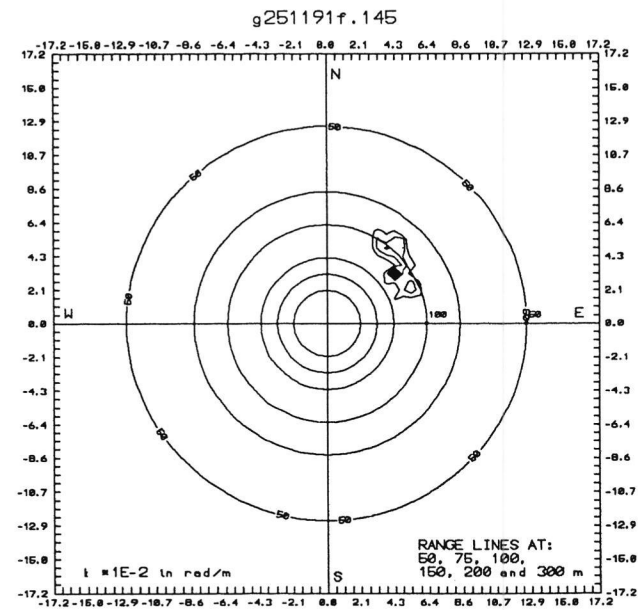
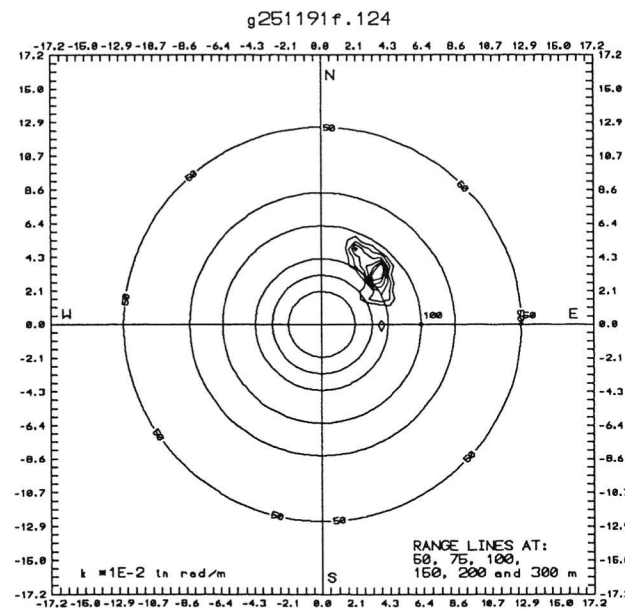
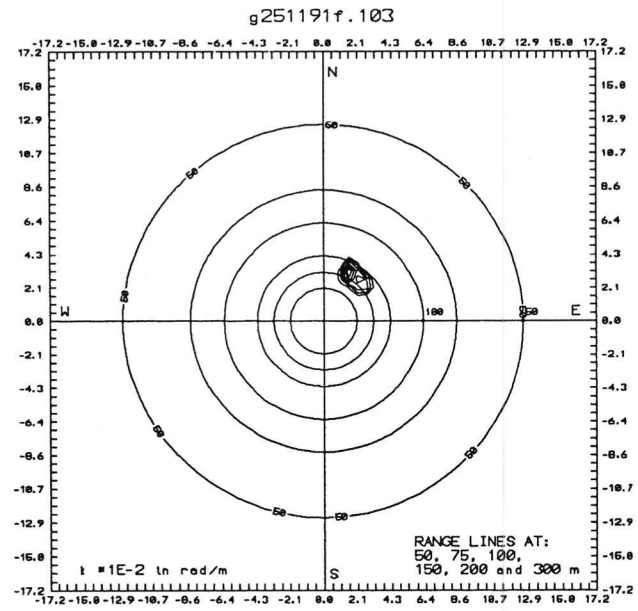
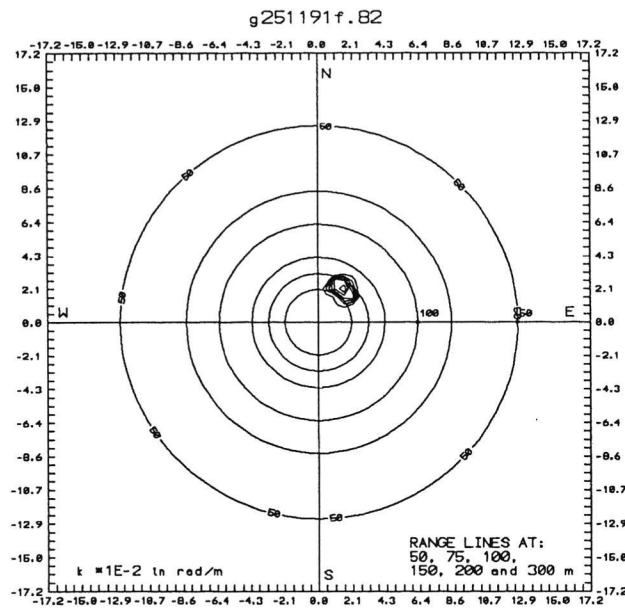
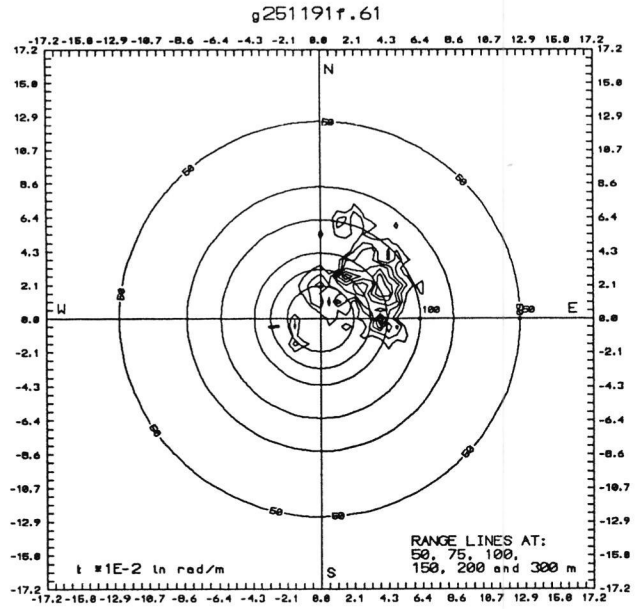
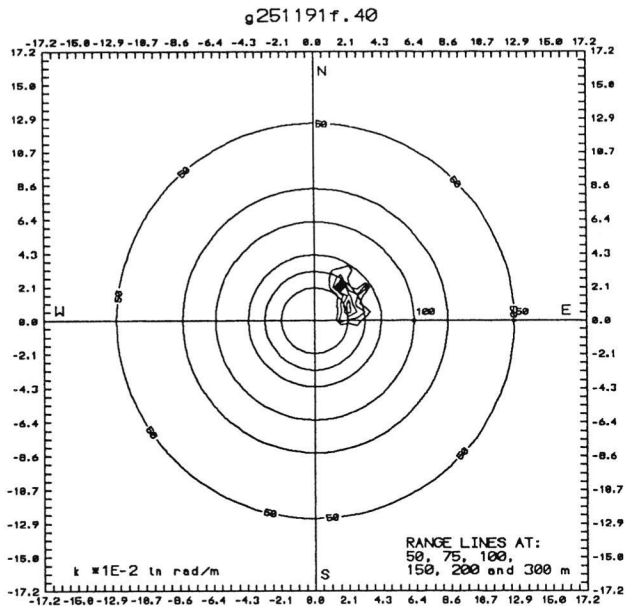


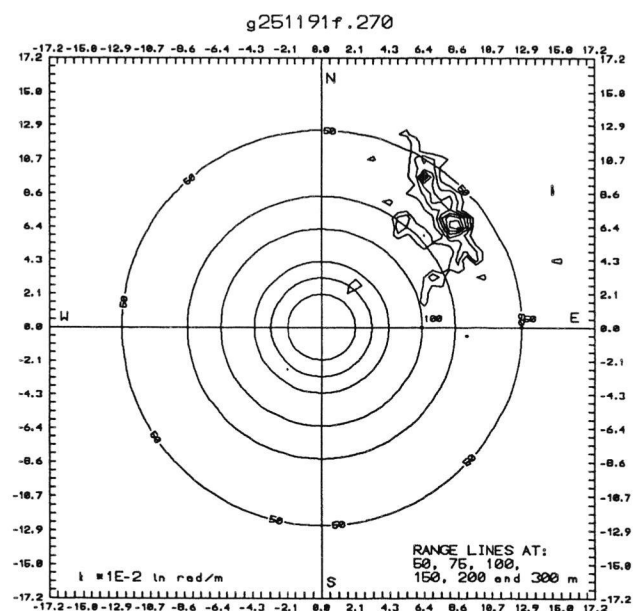
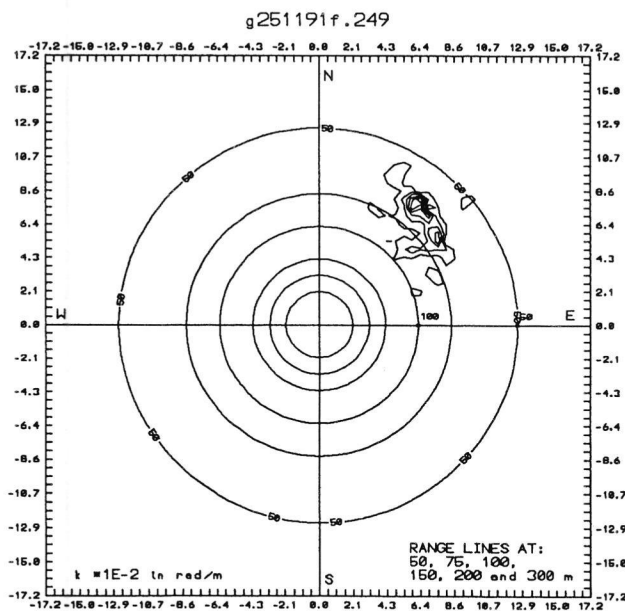
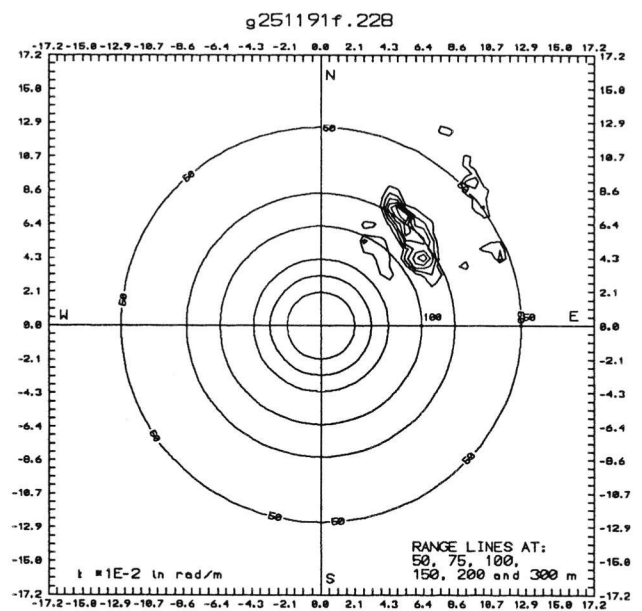
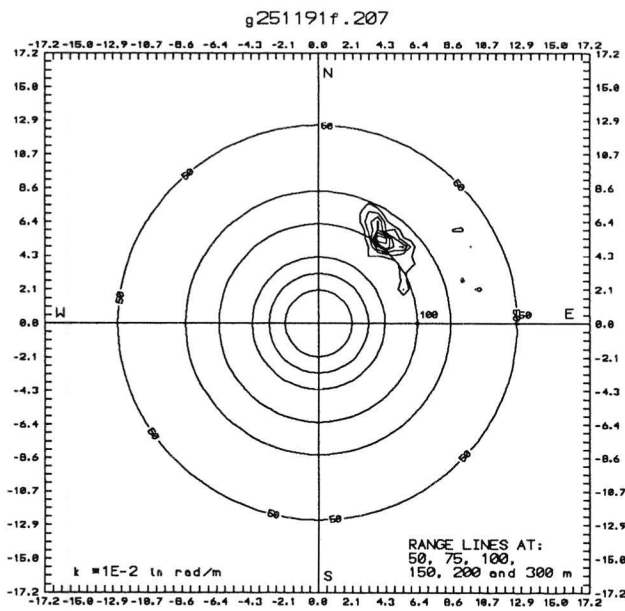
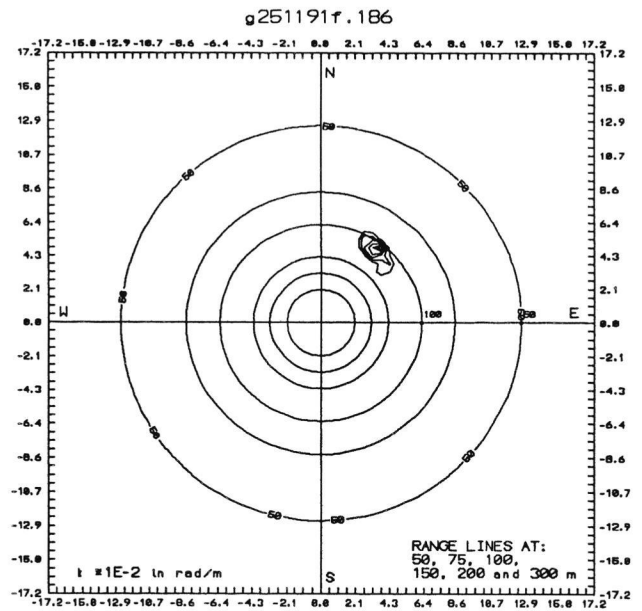
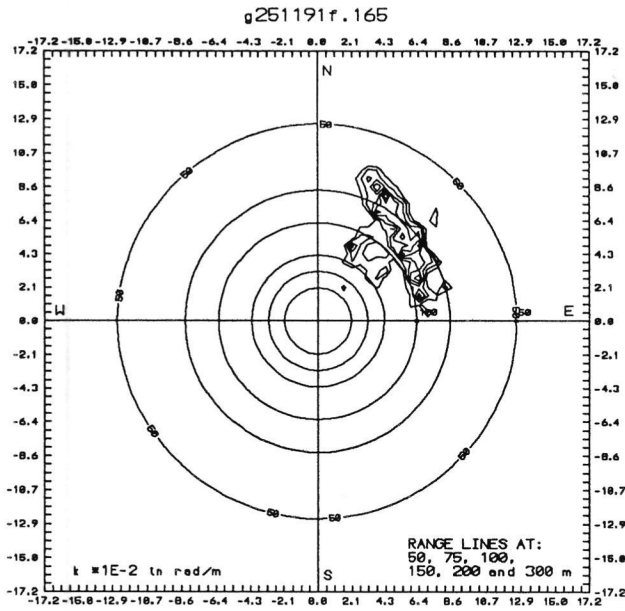


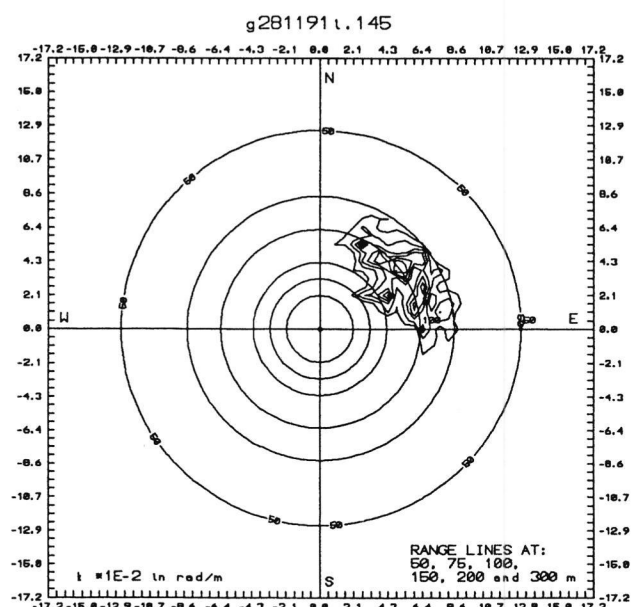
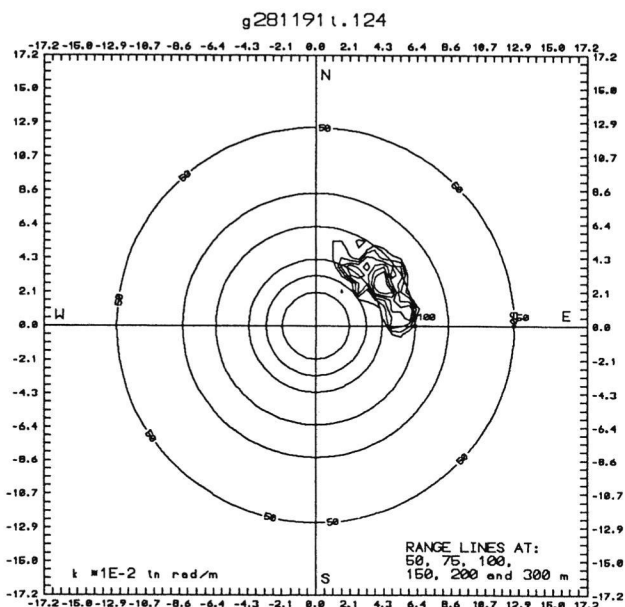
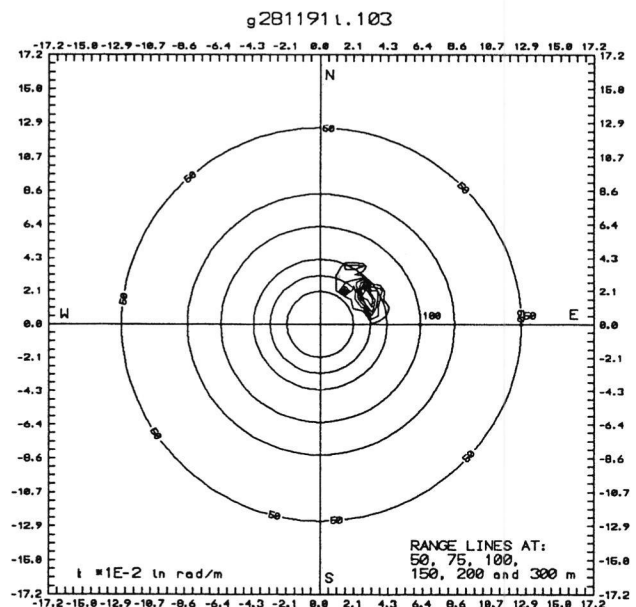
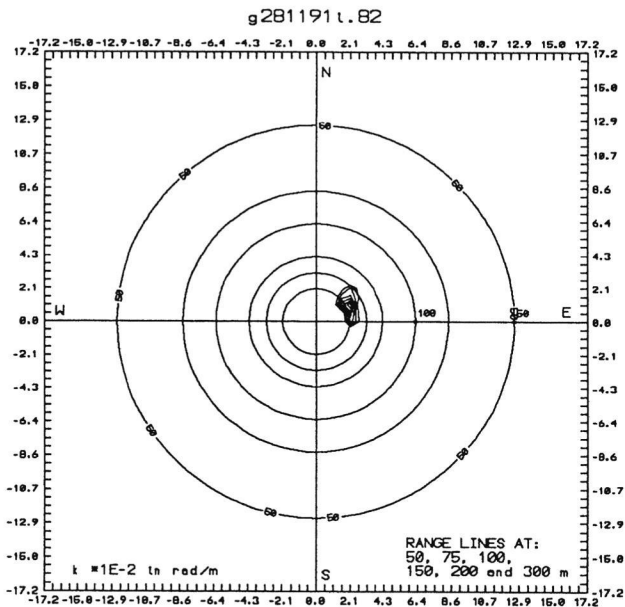
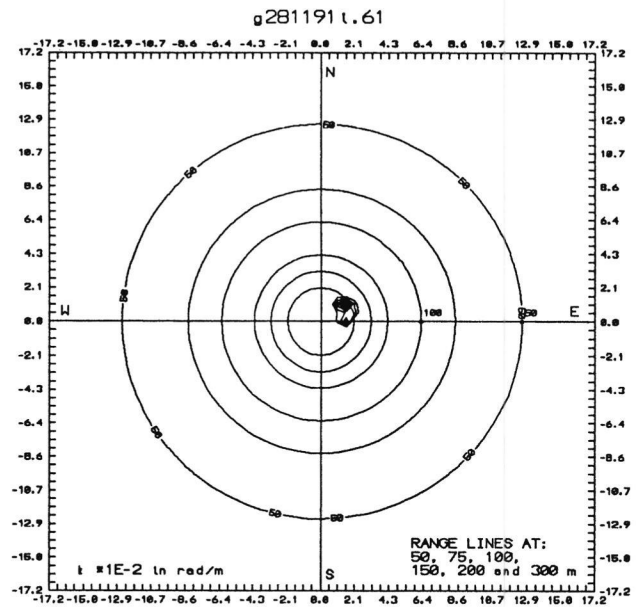
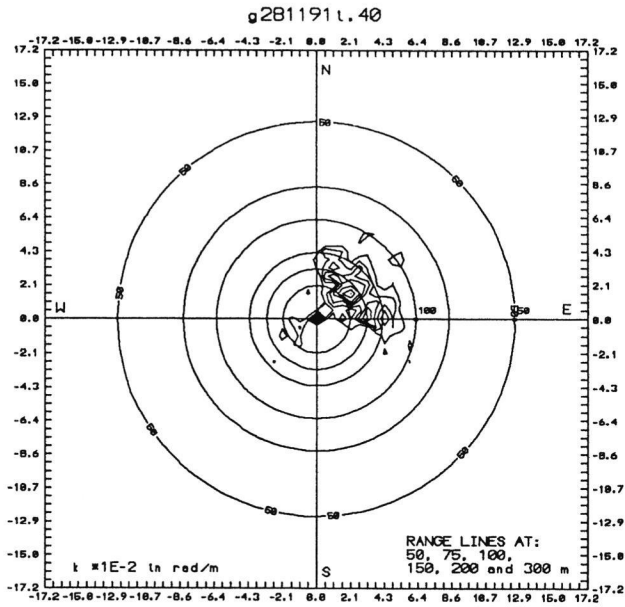












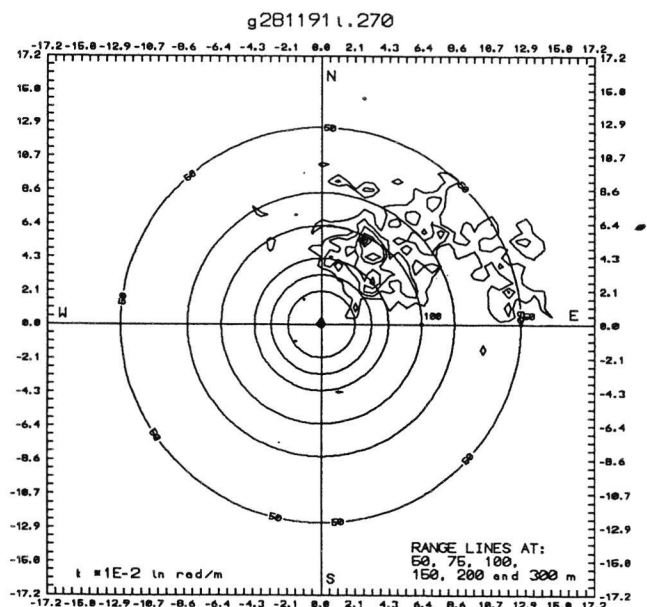
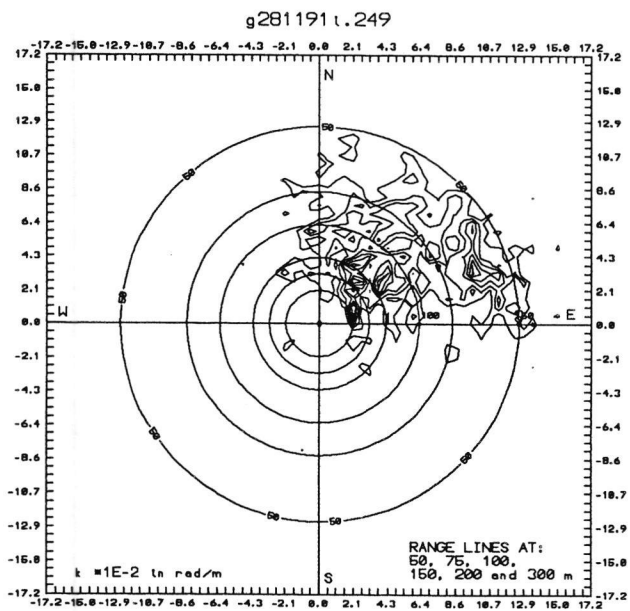
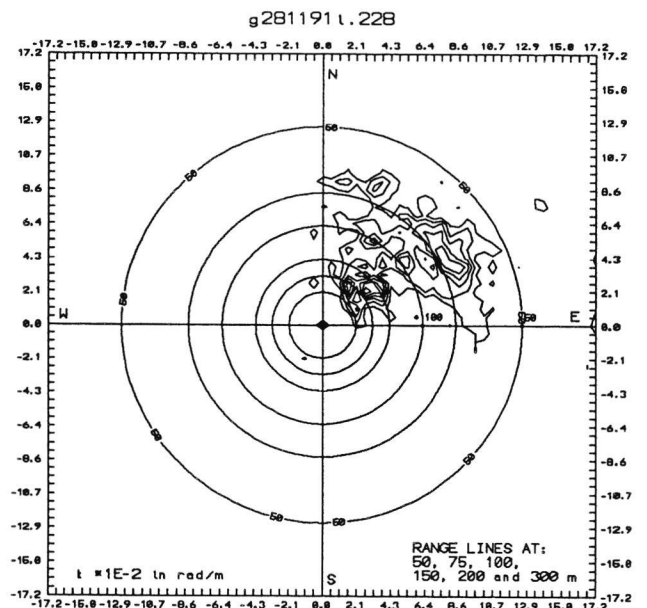
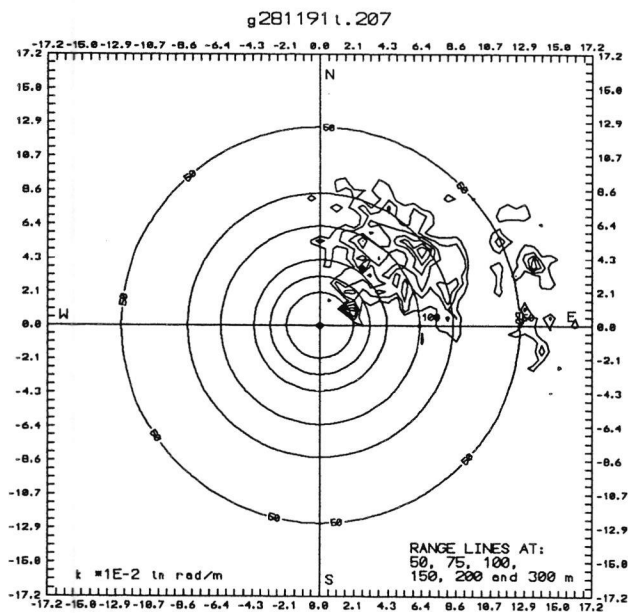
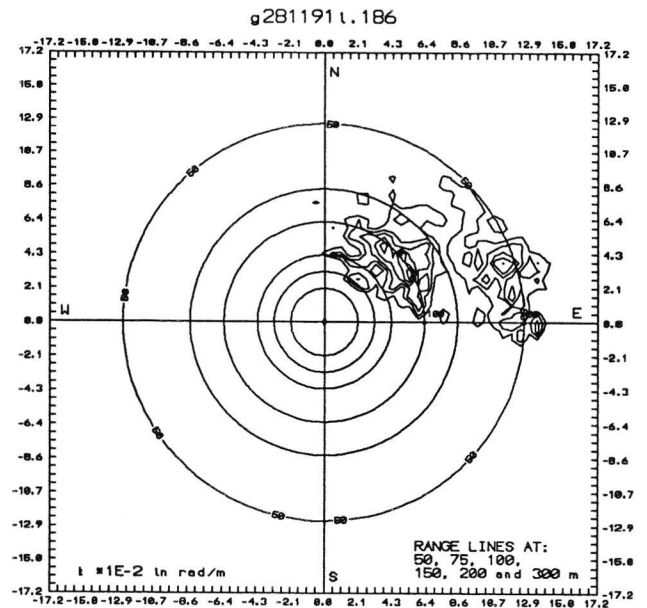
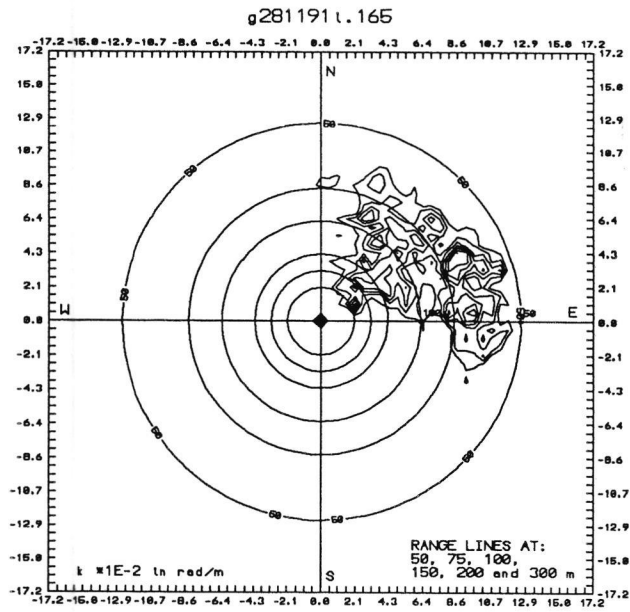
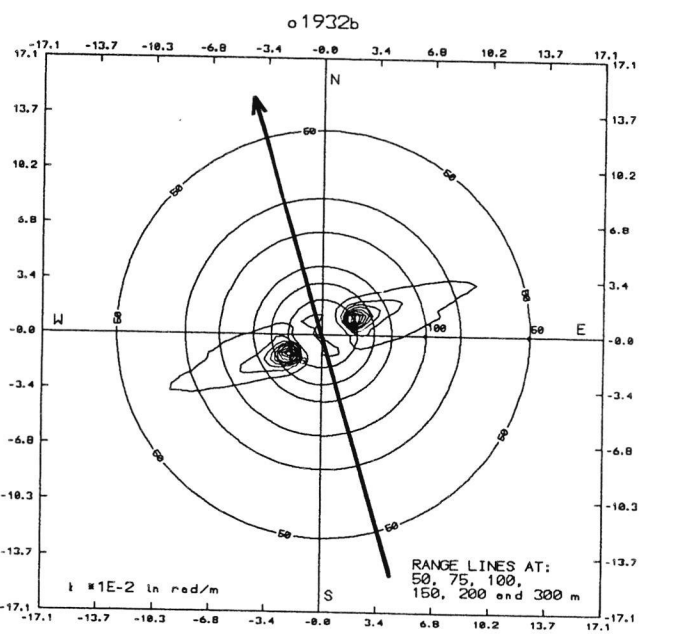
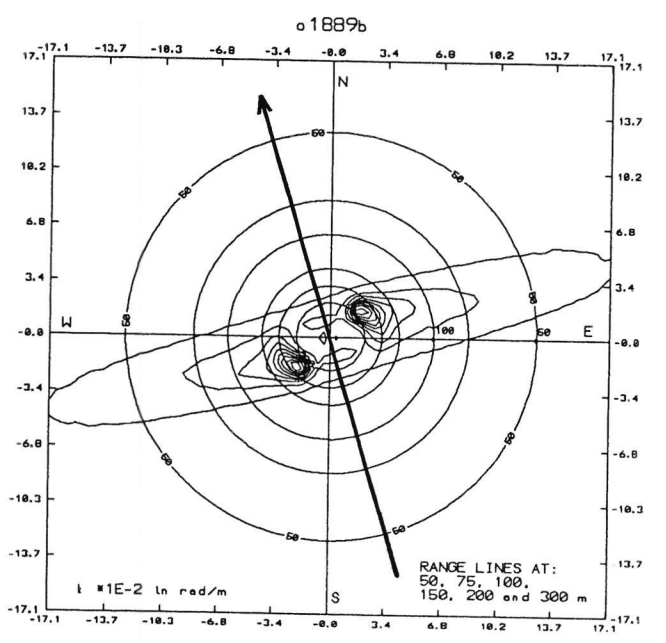
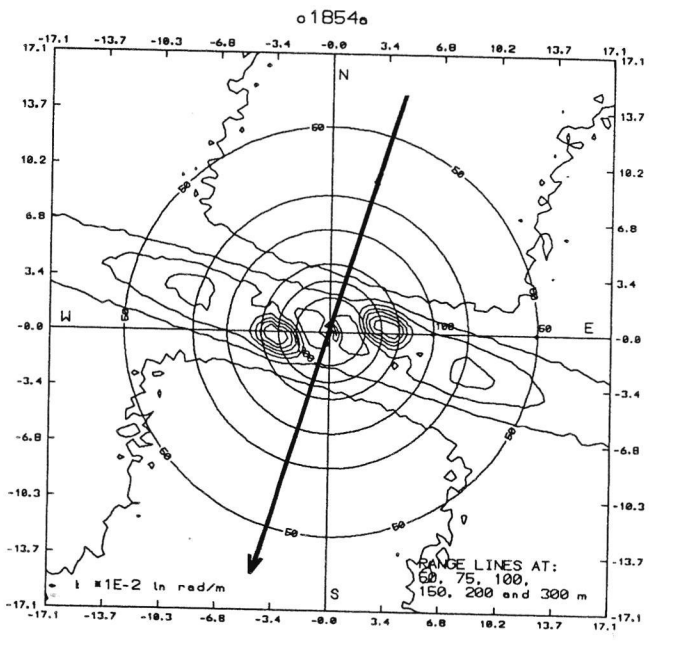
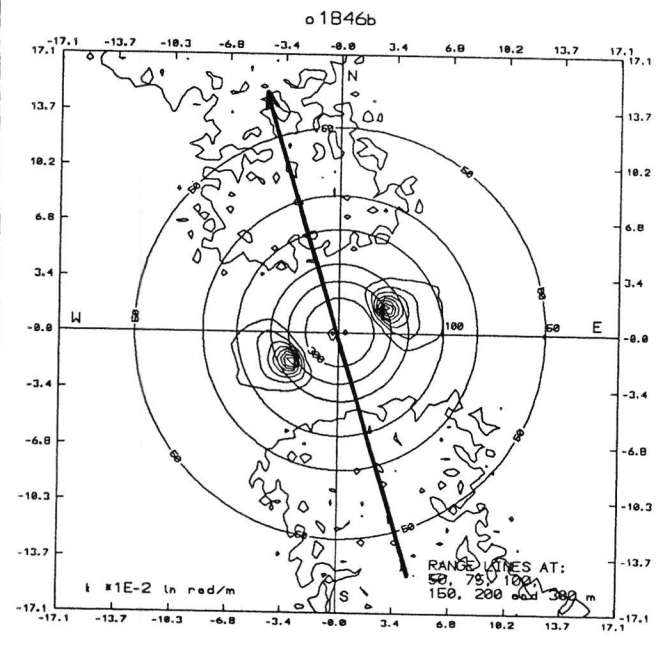
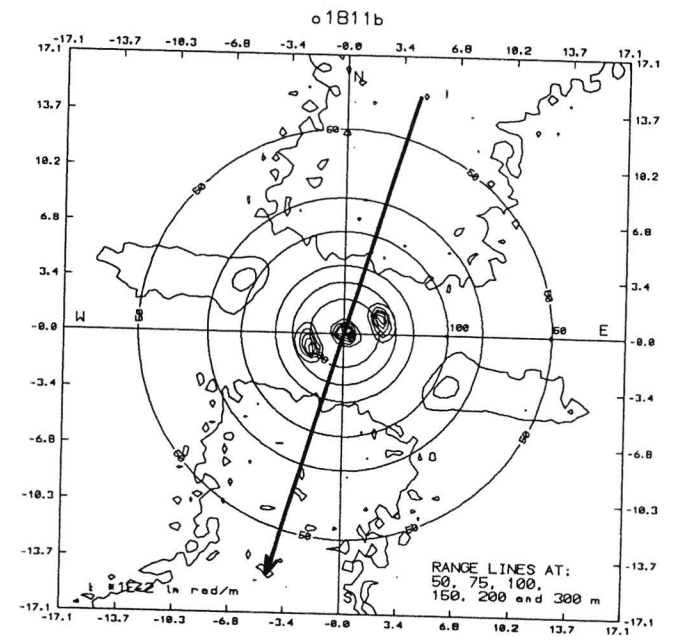
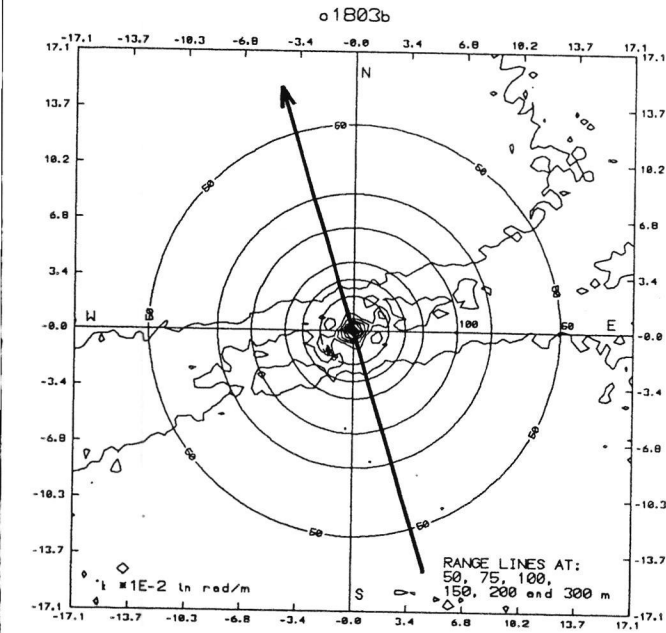
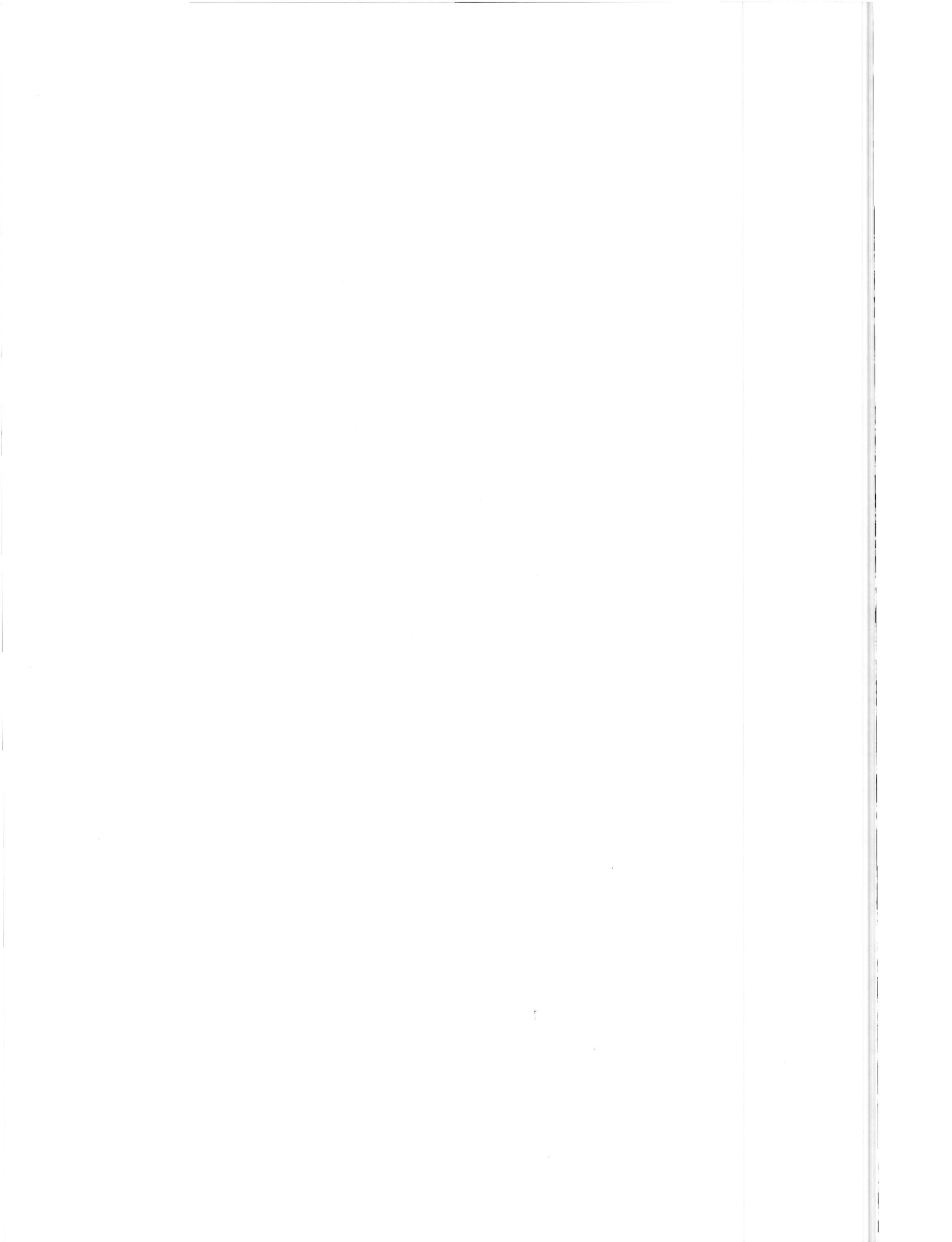
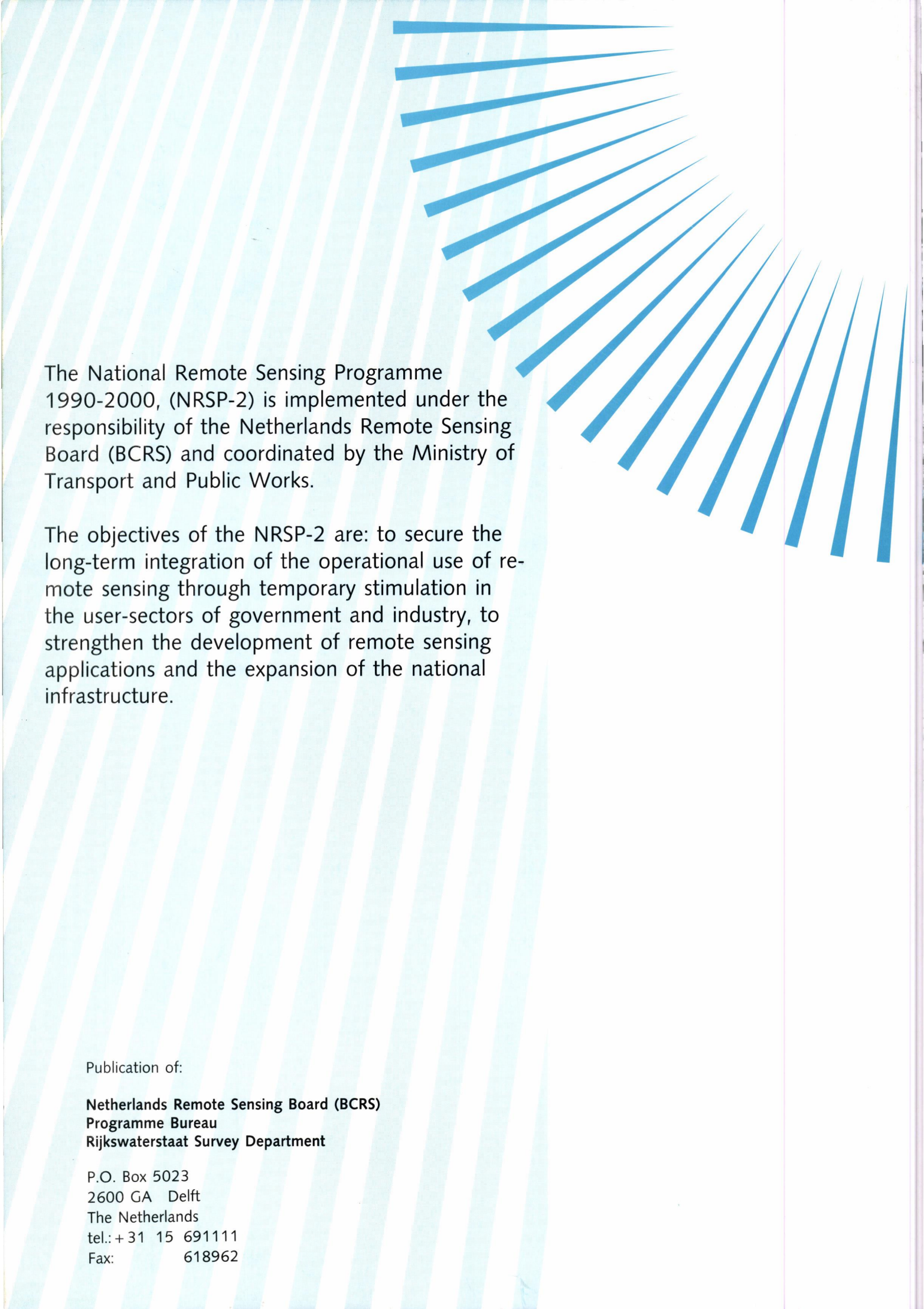


Figure 4 a-f (overleaf). ERS-1 directional wave spectra. The orbit number (ref. Table 1) is indicated on top of each spectrum. Contour spacing is relative to maximum. The azimuth direction is drawn in.









The National Remote Sensing Programme 1990-2000, (NRSP-2) is implemented under the responsibility of the Netherlands Remote Sensing Board (BCRS) and coordinated by the Ministry of Transport and Public Works.

The objectives of the NRSP-2 are: to secure the long-term integration of the operational use of remote sensing through temporary stimulation in the user-sectors of government and industry, to strengthen the development of remote sensing applications and the expansion of the national infrastructure.

Publication of:

**Netherlands Remote Sensing Board (BCRS)  
Programme Bureau  
Rijkswaterstaat Survey Department**

P.O. Box 5023  
2600 GA Delft  
The Netherlands  
tel.: +31 15 691111  
Fax: 618962